EPOS™ Electronic Presentation Online System

ESR European Society of Radiology

DW-MRI in detection and delineation of rectal cancer local recurrence

Poster No.:	C-2008
Congress:	ECR 2013
Type:	Scientific Exhibit
Authors:	S. Balyasnikova, E. Dronova, M. Dolgushin, A. Polynovskiy, D. Kuzmichev, B. Dolgushin; Moscow/RU
Keywords:	Oncology, Colon, Pelvis, MR-Diffusion/Perfusion, MR, Diagnostic procedure, Imaging sequences, Tissue characterisation
DOI:	10.1594/ecr2013/C-2008

Purpose

Improvement of rectal cancer management and new treatment options led to gradual decrease in locally recurrent rectal cancer rates; however relapse is still reported to occur in 15-35% of patients following rectal cancer surgery [1-4]. Majority of relapses occur within two years following rectal cancer surgery and three-fourths within 5 years [4-5].

Abdominopelvic pain is the most frequent presenting symptom and together with CEA levels rise is a reliable, but not an unreserved indication of rectal cancer local recurrence. However assessment of CEA levels alone is not adequate follow-up as recurrence may occur in the absence of CEA lift, but identification of local recurrence before symptomatology may allow earlier and more effective treatment [6].

It has already been shown that MRI is the best modality for rectal cancer patients follow-up [7-13], however standard sequences not always allow to differentiate fibrotic tissue from tumor relapse areas, thus makes it difficult not only to detect local recurrence at the initial stage of the disease but also to evaluate response of the relapse tumor to the received therapy.

In our study we tried to assess Diffusion-weighted MR feasibilities in identification and delineation of rectal cancer local recurrence.

Methods and Materials

Fifteen patients with previously treated rectal cancer were included in the study. There were 7 males and 8 females (mean age 54,8; range from 33 to 79 years). Three patients suffered from planocellular carcinomas of the anus, 12 patients were previously diagnosed and treated for rectal adenocarcinomas. Fourteen patients underwent surgery treatment, so that 2 APE (abdomino-pelvic extirpation), one#artmann's surgery and 11 TME (total mesorectal excision) were performed, in one case surgery treatment was omitted due to no tumor presentation after neoadjuvant treatment. All of the patients included in the study received either neoadjuvant or adjuvant (radio- or combined chemoradio therapy).

MRI scans to all of the patients were performed on 1,5 T scanners (Avanto/Espree, Siemence, Germany) with standard pelvic MRI protocol included: T2 cor (large FOV, 4 mm), T2 sag (small FOV, 4 mm), T2 tra (small FOV, 3 mm), DWI with identical parameters to T2 tra images (b value 0,800,1000 c/mm^2) and automatic ADC maps reconstructions. After sequential reading of all the images, we fused T2 tra and DW images (b value 1000 c/mm^2), T2 tra and ADC maps (on MultiModality Workstation, Siemens) and assessed results interpretation confidence.

Results

After complex diagnostic examination, no recurrent disease was identified in three patients, other 12 patients had relapse either at sites of sutural lines or extraintestinal pelvic compartments (involvement of any pelvic region); 8 % of patients developed recurrence in three month period after surgery, in 58,7% relapse occurred within a year and 33,3% had recurrence in 1,5-2 years period. From those with relapse disease blood cancer markers testes showed rise in 70% of cases.

Areas of tumor presence had intermediate SI (signal intensity) on T2 images, hyperintense areas on DWIs with b values of 800 and 1000 c/mm^2, and low SI areas on ADC maps. Since limited spatial resolution of high b values DW images and artifacts from bowel, free fluid collections (etc.) could cause difficulties in imaging interpretation, we noted that it was much easier to depict and differentiate tumor areas from either edema or fibroses on fused T2-DW images compared with separate reading of both sequence images. In the majorly of cases fused T2/DW images helped us to overcome some imaging reading problems, thus providing more accurate information about tumor presence and spread to adjacent organs and pelvic structures; so that imaging accuracy increased from 65% up to 87% (in each case patient had either biopsy of suspicious region or surgical excision of the relapse tumor with postoperative specimen histological examination). Those patients who were considered as inoperable at the moment of initial examination, received either radio-, chemo-, or combined radiochemotherapy and had follow-up MRI scans with the same protocols and scanning parameters.

We counted ADC values for all the tumor zones seen on the fused T2 axial/DW images, however could not sort out precise threshold values for tumor presence. Residual tumor areas had heterogeneous SI (signal intensity) on T2 and showed multivendor average ADC values (from 850+/-50 to 2000+/-50) (pic. 1), so that we could not suggest using ADC index as a reliable marker of recurrence identification; however ADC maps could help in assessment of relapse tumor response to treatment (pic. 2). Fibrotic tissue formation at the sites of previously seen tumor corresponded with average ADC values decrease. We could not note any significant difference in ADC values between patient groups with different pre- and post treatment therapy regimes. Three patients also underwent PET-CT examination (pic. 3), in all cases results agreed with DW-MRI findings.

Images for this section:

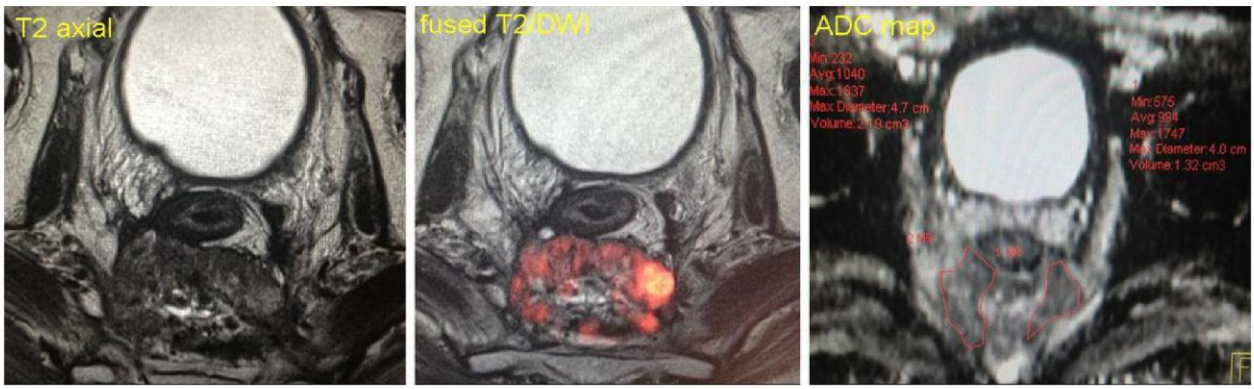

Fig. 1: A 38-year-old patient had TME for middle rectal cancer treatment. Within 6 month period relapse disease was diagnosed. T2 image shows heterogeneous tumor tissue, that involves posterior pelvic compartment. Heterogeneous tumor structure is also displayed on fused T2/DWIs and ADC maps (with different ADC index).

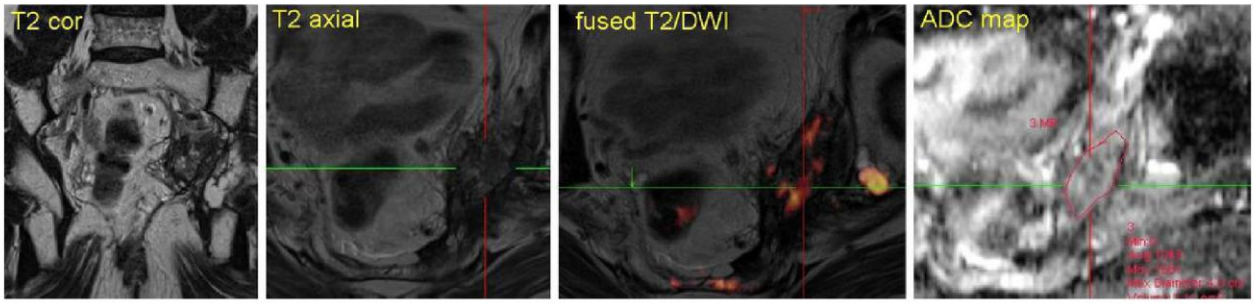

Fig. 2: A 65-year-old patient was surgically treated for low rectal adenocarcinoma (TME) in 2010, developed recurrence disease in 2012. (pic. 2) Initial MRI scan, T2 images demonstrate hypo/isointense tumor node next to left pelvic side wall, which infiltrating obturator internus m, left seminal vesicle, muscular fascicles of the left piriformis m. On fused T2/DWI tumor recurrence zone shows high SI. Average ADC index is 1040. (pic. 3,4) Follow-up scans were made during (3) and after (4) chemoradiotherapy. Increase in fibrotic tissue formation is seen on T2 images with correspondent loss of high SI on fused images and decrease of ADC parameter.

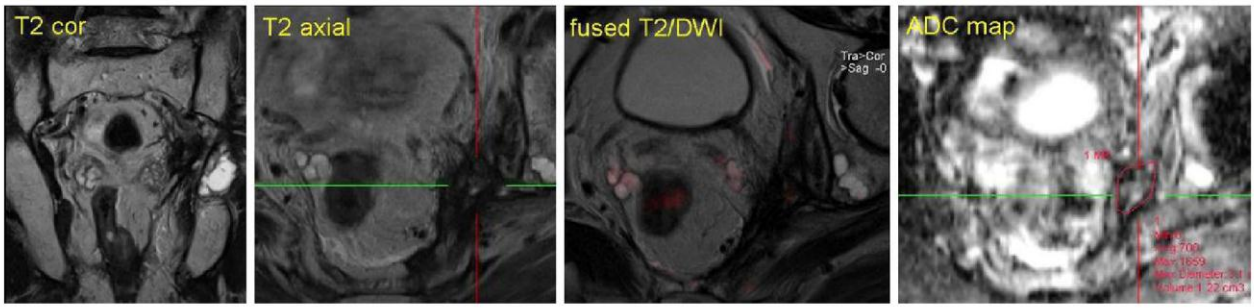

Fig. 3: A 65-year-old patient was surgically treated for low rectal adenocarcinoma (TME) in 2010, developed recurrence disease in 2012. (pic. 2) Initial MRI scan, T2 images

demonstrate hypo/isointense tumor node next to left pelvic side wall, which infiltrating obturator internus m, left seminal vesicle, muscular fascicles of the left piriformis m. On fused T2/DWI tumor recurrence zone shows high SI. Average ADC index is 1040. (pic. 3,4) Follow-up scans were made during (3) and after (4) chemoradiotherapy. Increase in fibrotic tissue formation is seen on T2 images with correspondent loss of high SI on fused images and decrease of ADC parameter.

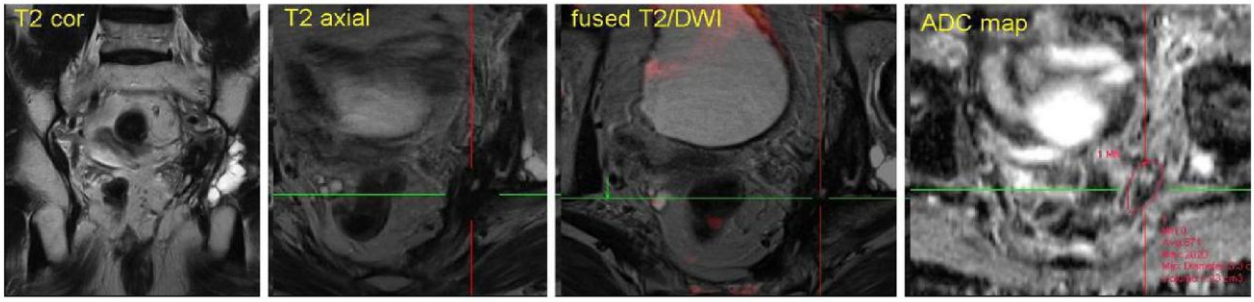

Fig. 4: A 65-year-old patient was surgically treated for low rectal adenocarcinoma (TME) in 2010, developed recurrence disease in 2012. (pic. 2) Initial MRI scan, T2 images demonstrate hypo/isointense tumor node next to left pelvic side wall, which infiltrating obturator internus m, left seminal vesicle, muscular fascicles of the left piriformis m. On fused T2/DWI tumor recurrence zone shows high SI. Average ADC index is 1040. (pic. 3,4) Follow-up scans were made during (3) and after (4) chemoradiotherapy. Increase in fibrotic tissue formation is seen on T2 images with correspondent loss of high SI on fused images and decrease of ADC parameter.

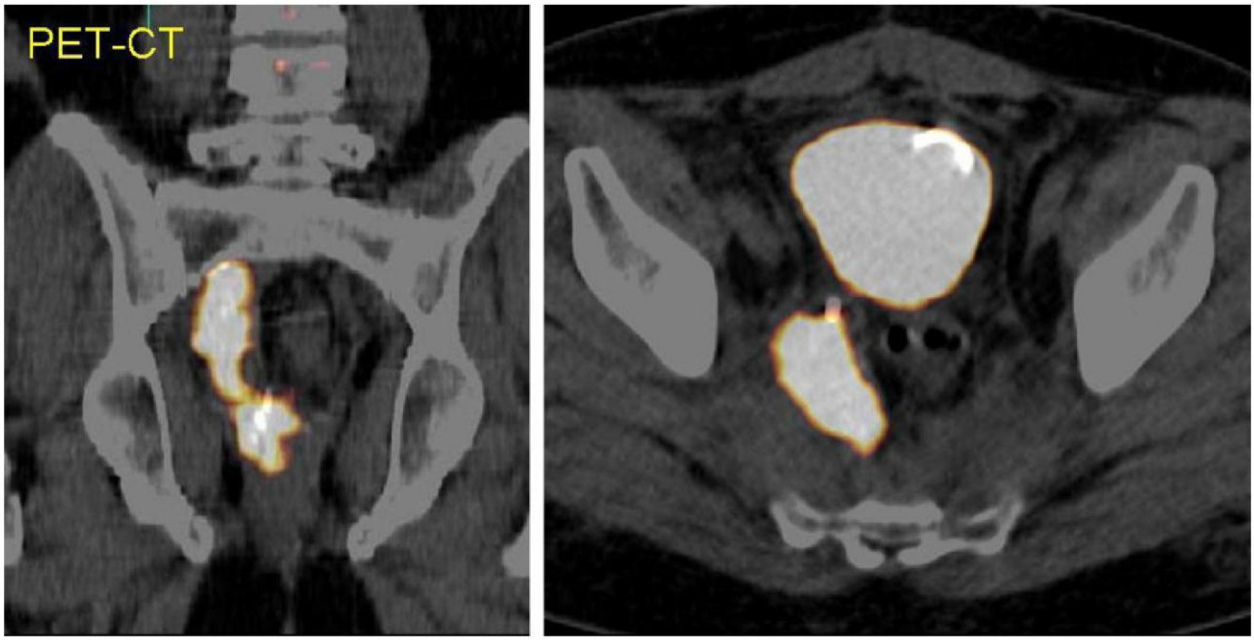

Fig. 5: A 60-year-old patient developed rectal cancer relapse in a year period after neoadjuvant and surgery treatment of the primary rectal tumor. (pic. 5) PET-CT scans

show right pelvic side zone of increased 18-FDG uptake. (pic. 6) MR T2 image depicts low/intermediate SI tumor area, involving right lateral and anterior pelvic compartments, with posterior bladder wall and right ureter infiltration (due to native soft tissue contrast MRI clearly identifies relation of tumor tissue to adjacent organs). Fused T2/DWI displays tumor as high SI area, opposite to fused T2/ADC maps, where tumor is seen as low SI zones.

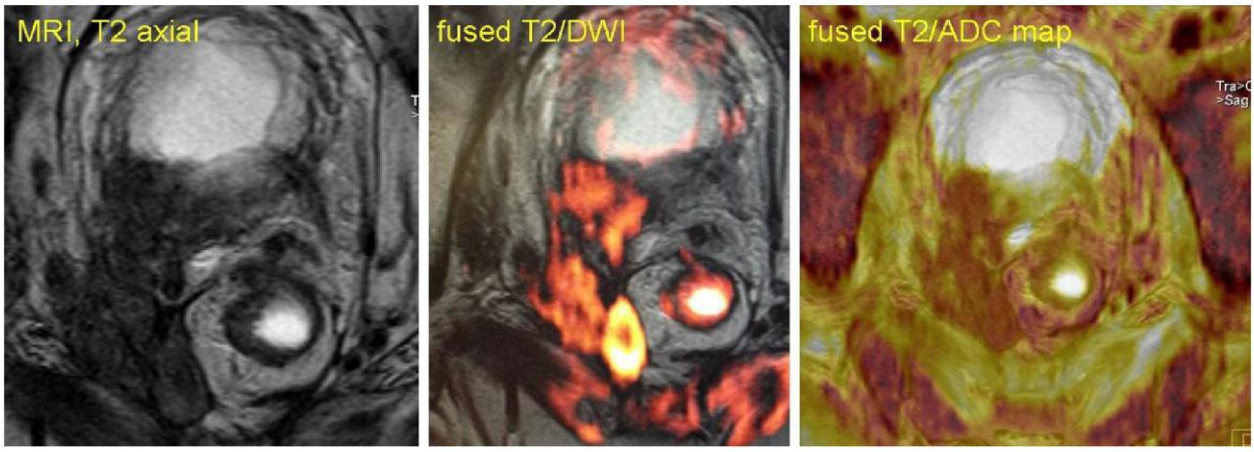

Fig. 6: A 60-year-old patient developed rectal cancer relapse in a year period after neoadjuvant and surgery treatment of the primary rectal tumor. (pic. 5) PET-CT scans show right pelvic side zone of increased 18-FDG uptake. (pic. 6) MR T2 image depicts low/intermediate SI tumor area, involving right lateral and anterior pelvic compartments, with posterior bladder wall and right ureter infiltration (due to native soft tissue contrast MRI clearly identifies relation of tumor tissue to adjacent organs). Fused T2/DWI displays tumor as high SI area, opposite to fused T2/ADC maps, where tumor is seen as low SI zones.

Conclusion

DW-MRI has already shown its feasibility in rectal cancer complete responders detection and is widely used in oncology imaging [13-15]. Rectal cancer recurrence is a difficult to treat condition; its earlier identification could help to increase overall survival of colorectal cancer patients. DW-MRI could be considered as quiet a reliable imaging modality for colorectal cancer recurrence, but more studies should be carried out.

References

1. Manfredi, S. and Benhamiche, A. "Population-Based Study of Factors Influencing Occurrence and Prognosis of Local Recurrence after Surgery for Rectal Cancer." British Journal of Surgery 88.9 (Nov. 2002): 1221-1227. Wiley InterScience. 21 Aug. 2006.

2. Temple WJ, Saettler EB. Locally recurrent rectal cancer: role of composite resection of extensive pelvic tumors with strategies for minimizing risk of recurrence. J Surg Oncol 2000;73:47-58.

3.Quirke P, Durdey P, Dixon MF, Williams NS Local recurrence of rectal adenocarcinoma due to inadequate surgical resection. Histopathological study of lateral tumour spread and surgical excision. Lancet 2 1986; 8514:996-999.

4.Fuzun M, Terzi C, Sokmen S, Unek T, Haciyanli M. Potentially curative resection for locoregional recurrence of colorectal cancer. Surg Today. 2004;34:907-912.

5.Obrand D, Gordon P. Incidence and patterns of recurrence following curative resection for colorectal carcinoma. Dis Colon Rectum. 1997;40:15-24.

6. Steele G. Standard postoperative monitoring of patients after primary resection of colon and rectum cancer. Cancer. 1993;71:4225-4235.

7.Brown G, Davies S, Williams GT et al. Effectiveness of preoperative staging in rectal cancer: digital rectal examination, endoluminal ultrasound or magnetic resonance imaging? Br J Cancer. 2004;91 (1):23-29.

8. Christian K, Patrik R, Matthias T. Local staging of rectal cancer: the current role of MRI. Eur Radiology (2007) 17:379-389.

9. Gina B. Rectal carcinoma staging: a practical approach. RSNA 2010.

10. Gina B. thin section MRI in multidisciplinary pre-operative decision making for patients with rectal cancer. The British Journal of Radiology, 78 (2005), S117-S127.

11. MERCURY Study Group. Diagnostic accuracy of preoperative magnetic resonance imaging in predicting curative resection of rectal cancer: prospective observational study. BMJ 2006; 333(7572):779.

12. Schaefer O, Langer M. Detection of recurrent rectal cancer with CT, MRI and PET/CT. Eur Radiol. 2007 Aug;17(8):2044-54. Epub 2007 Apr 3.

Katsuhiro N, Yoshihumi K, Seiko K, Koji M, Shigeru N, Noriyuki M. Diffusion-weighted signal shot echo planar imaging of colorectal cancer using a sensitivity-encoding technique. Jpn J Clin Oncol 2004; 34 (10) 620-626.

13.Colosio A, Fornès P, Soyer P, Lewin M, Loock M, Hoeffel C. Local colorectal cancer recurrence: pelvic MRI evaluation. Abdom Imaging. 2013 Feb;38(1):72-81. doi: 10.1007/s00261-012-9891-5.

14. Seung H, Jeong M, Sung H, Gi H, Jae Y, Joo K, Byung I. Locally advanced rectal cancer: added value of diffusion-weighted MR imaging in the evaluation of tumor response to neoadjuvant chemo- and radiation therapy. RSNA, Radiology: volume 253: number 1, 2009.

15. Doenja M, Vincent V, Brunella B, Frans C, Maarten L, Monique M, Karin H, Vincenzo V, Geerard L, Regina G. Diffusion-weighted MRI for selection of complete responders after chemoradiation for locally advanced rectal cancer: a multicenter study. Ann Surg Oncol (2011) 18:2224-2231.

Personal Information

ПОСТЕР

Biliary complications of liver tumor chemoembolization

Poster No.:	C-2523
Congress:	ECR 2013
Type:	Scientific Exhibit
Authors:	O. N. Sergeeva, E. Virshke, I. Trofimov, A. V. Kukushkin, V. Panov, B. Dolgushin; Moscow/RU
Keywords:	Outcomes, Cancer, Abscess, Outcomes analysis, Cholangiography, Chemoembolisation, MR, Catheter arteriography, Liver, Biliary Tract / Gallbladder, Abdomen
DOI:	10.1594/ecr2013/C-2523

Purpose

The main idea of hepatic transcatheter arterial chemoembolization (TACE) proposed in 1980-s is selective liver tumor treatment by chemotherapy/ischemia combination due to the principle arterial supply of the neoplastic tissue while the rest of the hepatic parenchyma has 80% portal and 20% arterial perfusion [1]. The only hepatic structures with intrinsic dominant arterial supply are the bile ducts [2] (Figure 1). The post-TACE bile duct injury is to be accessed.

Images for this section:

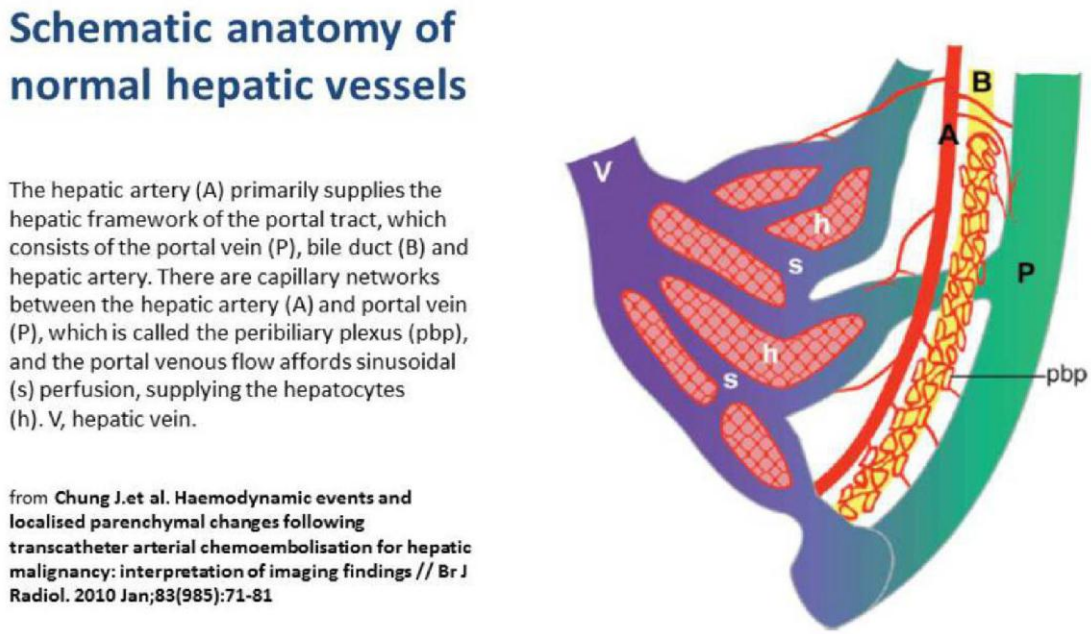

Fig. 1: Intrinsic dominant arterial blood supply of the bile ducts results in increased risk of post-TACE biliary injury.

Methods and Materials

Since 1994 301 patients have undergone 753 TACE procedures (mean 2.5 procedures per patient, range 1-13) in N.N. Blokhin Cancer Research Center for hepatic malignancies using iodized oil or drug eluting beads with varying chemotherapeutic drugs. TACE were performed to non-surgical candidates. Inefficiency or a lack of efficient systemic chemotherapy was evident for the majority of the patients. Chemoembolization technique included selective or superselective hepatic arteriography followed by insertion of chemoembolization compound (Figure 2). The prolonged elimination of iodized oil was confirmed by follow-up CT scans (Figure 3).

Post-procedural monitoring consisted of clinical examination, laboratory tests and visualization procedures (CT and MRI) with special note on biliary complications.

Images for this section:

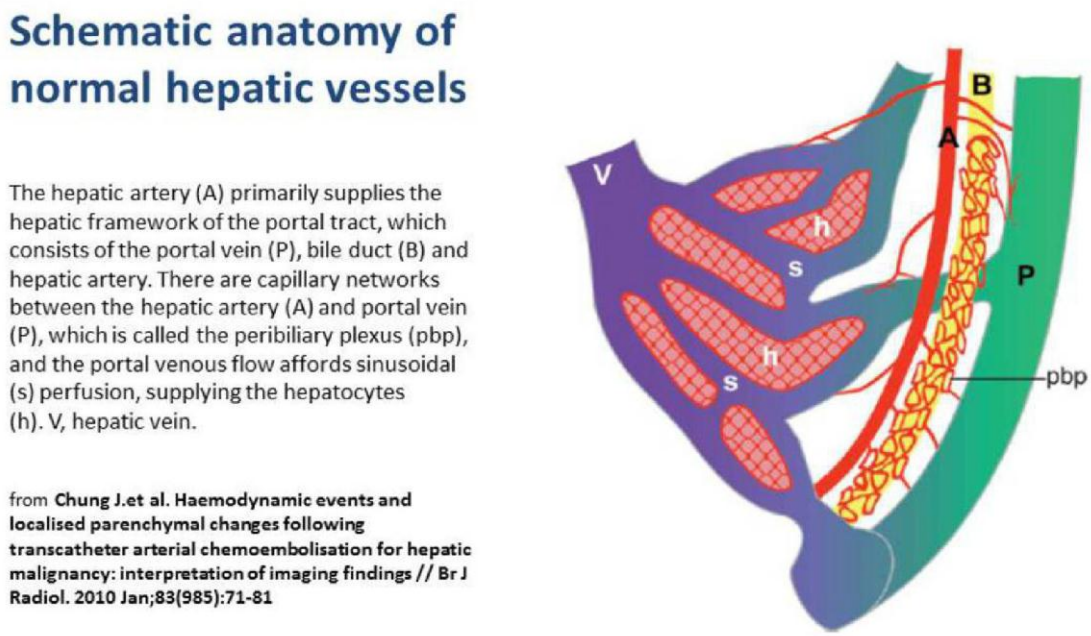

Fig. 1: Intrinsic dominant arterial blood supply of the bile ducts results in increased risk of post-TACE biliary injury.

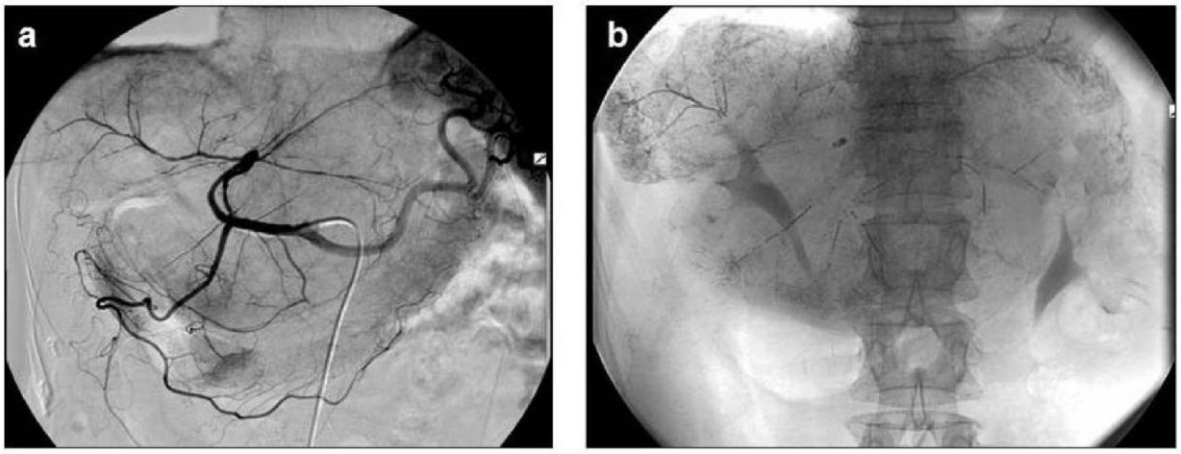

Fig. 2: TACE technique. Selective hepatic arteriography (a) followed by insertion of chemoembolization compound (mixture of iodized oil with doxorubicin)(b).

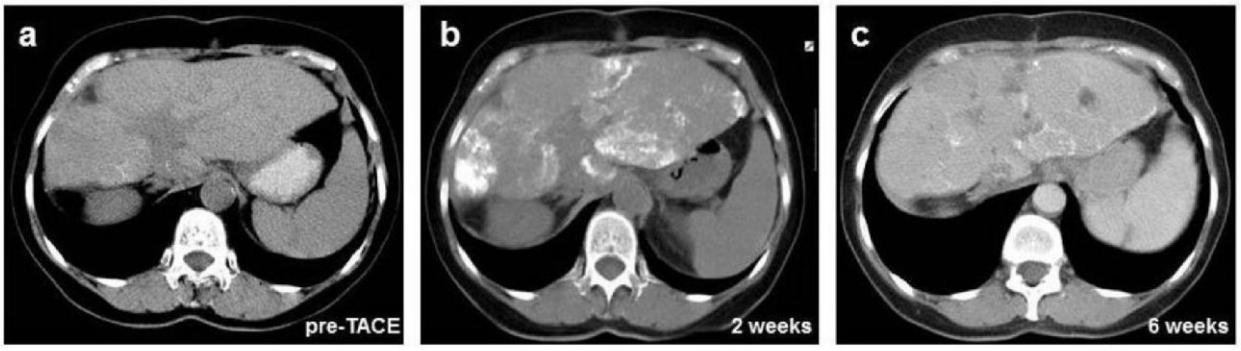

Fig. 3: Slow elimination of iodized oil. Pre-TACE CT (a), two (b) and six (#) weeks after TACE ##.

Results

Post-embolization cholangiopathy developed in 5 patients (3 male, 2 female, age range 32-65 years) underwent TACE for hepatocellular carcinoma - 2, cholangiocarcinoma - 2, skin melanoma liver metastases -1. Biliary complication rate was 1.7% per patient and 0.7% per procedure. Three out of five (3/5) patients had previously underwent major liver resection, one patient - nine preceding chemoembolization procedures during four years. The jaundice and fever occurred from 2 to 5 month after TACE procedure, visualization techniques revealed the biliary complications at the same time (Figure 4). MRI and CT findings were following: bile duct irregular dilatations and strictures (5), multiple post-necrotic bile duct cysts (4) (Figure 5), liver abscess (1) (Figure 6), regenerative nodules (1), ascites (1) (Figure 7). Three patients with previously resected liver died from 6 to 8 months after TACE due to liver failure. One patient was lost for follow-up.

One patient is alive for 12 months after TACE with bile duct strictures and irregular dilatations (Figure 8).

Several authors not unsuccessfully attempted to reveal correlations of TACE-induced bile duct injury with liver tumor type (hepatocellular carcinoma vs neuroendocrine metastases), embolization material (iodized oil versus drug eluting beads) or cirrhotic/ non-cirrhotic liver status [2-4]. In the paper we failed to identify any valuable biliary injury risk factor may be due to small number of cases. Pathophysiology of post-TACE bile duct complications wasn't clear enough. Simple ischemia? But why late manifestations then? The only notice seemed considerable to us. The preceding reducing hepatic arterial capacity treatments, e. g. hepatic resections, repeated TACE procedures, antiangiogenic therapies, etc., increased risk of post-TACE cholangiopathy. Three patients underwent major hepatic resection and one patient nine TACE procedures prior to bile duct injury complicated chemoembolization in the series. Poor played-out reserve of bile duct arterial supply remodeling appears the main possible TACE-induced biliary injury predilection.

Images for this section:

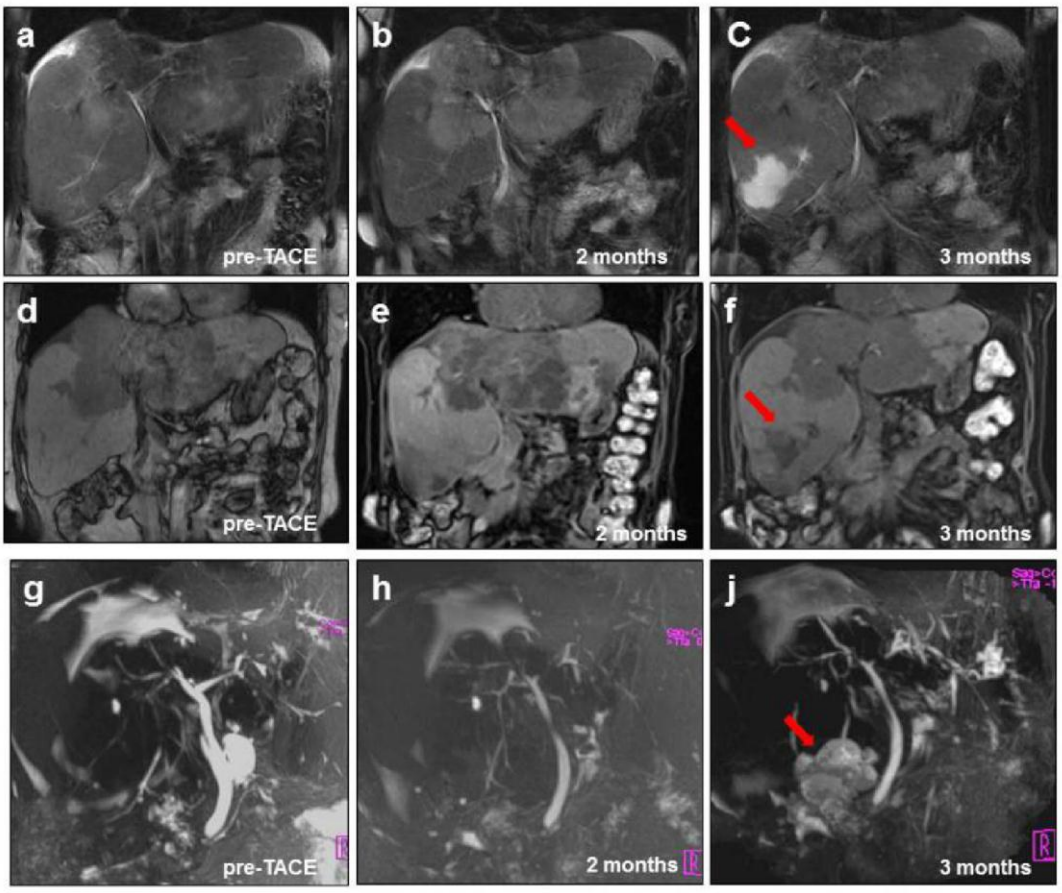

Fig. 4: Delayed manifestations of biliary complications. MRI of 65 years old female patient underwent TACE for cholangiocarcinoma: pre-TACE T2-WI (a), T1-WI (d), MRCP (g); two months after TACE T2-WI (b), T1-WI (e) demonstrating moderate heterogeneity of the six liver segment parenchyma only , MRCP (h); three months after TACE T2-WI (c), T1-WI (f) and MRCP (j) show postnecrotic bile duct cyst (arrow).

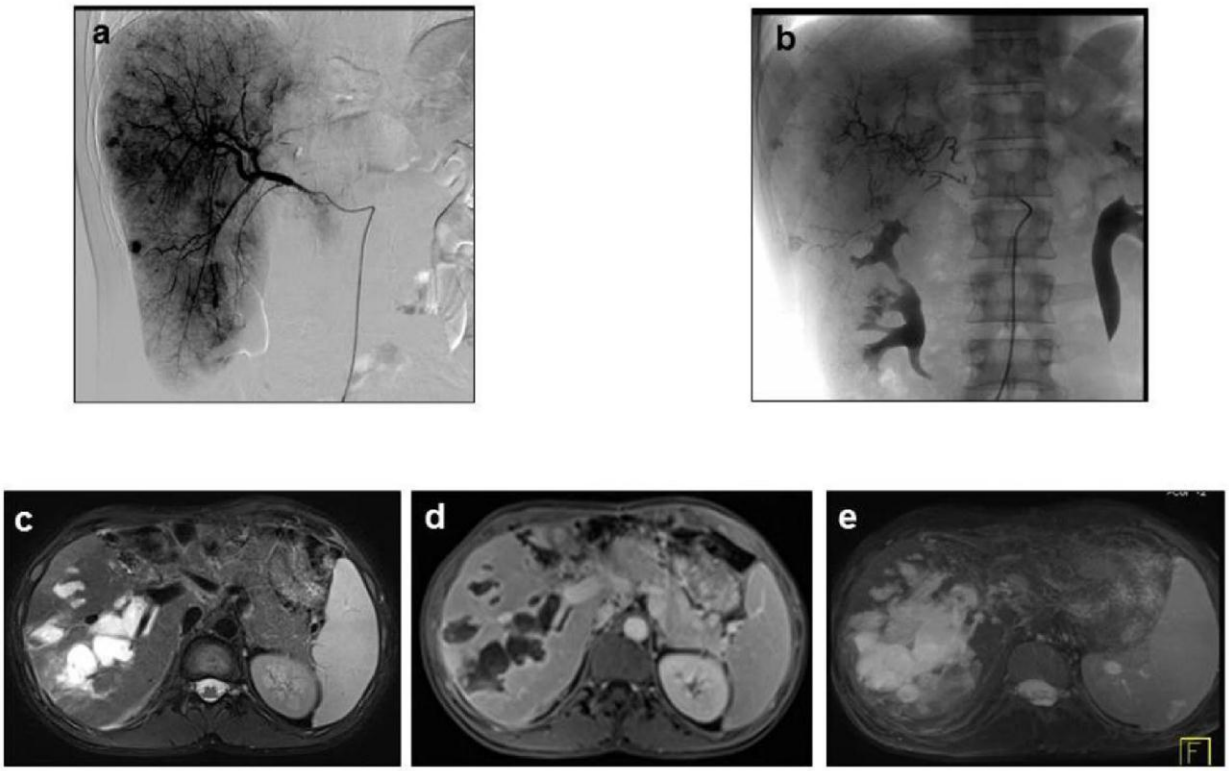

Fig. 5: Cystic transformation of bile ducts. 32 years old male hepatocellular carcinoma patient underwent TACE for multiple recurrent tumors in the liver remnant: (a) hepatic arteriography, (b) accumulation of the iodized oil in the right liver lobe. MRI two months after TACE: T2-WI (c), contrast enhanced T1-WI (d) and MIP (e) demonstrate almost totally cystic dilated bile ducts, periductal edema and hepatic parenchyma inflammation.

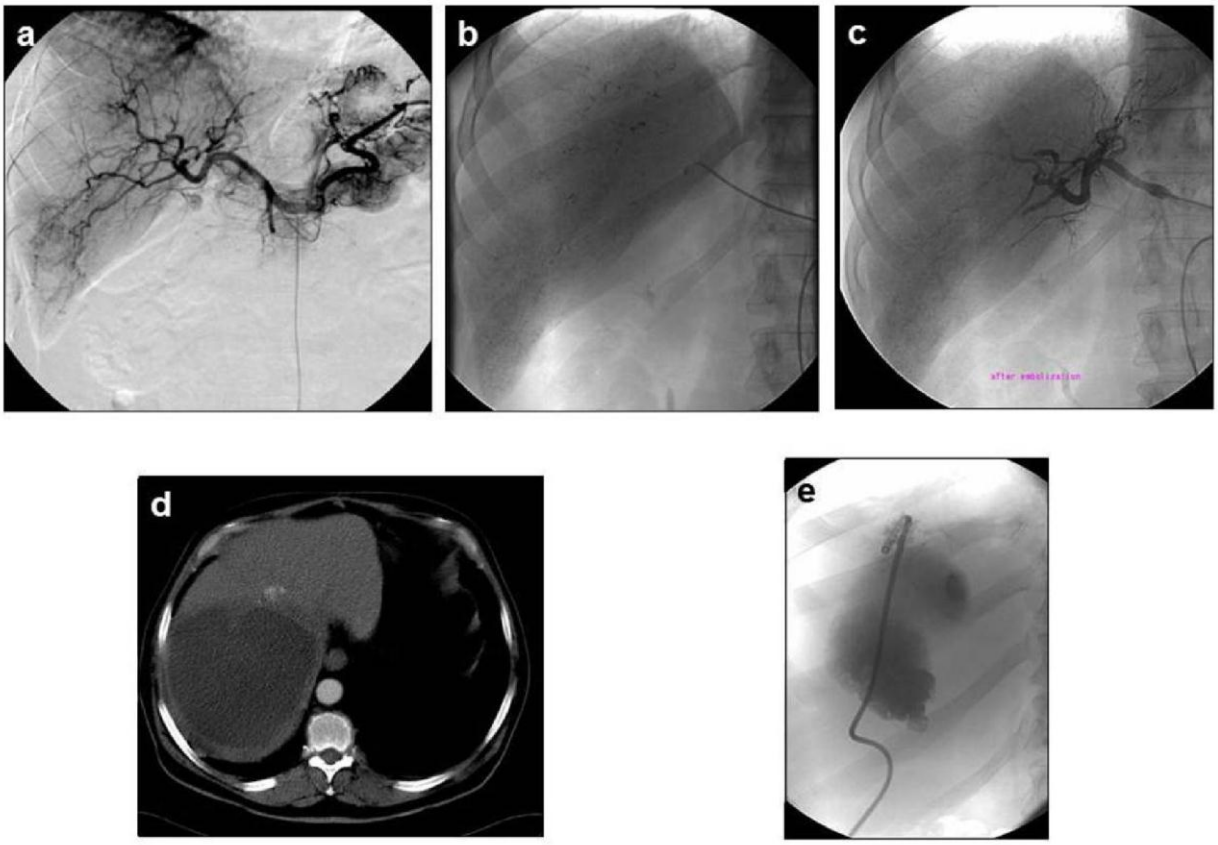

Fig. 6: Liver abscess. 63 years old male hepatic metastatic melanoma patient underwent 'dense' chemoembolization with iodized oil and carboplatin: (a) hepatic arteriography, (b) accumulation of iodized oil in the liver, (c) absence of blood flow in the peripheral hepatic arteries confirmed by post-TACE arteriography. CT (d) two months after TACE revealed right lobe liver abscess requiring percutaneous drainage (e) with bile fistula formation.

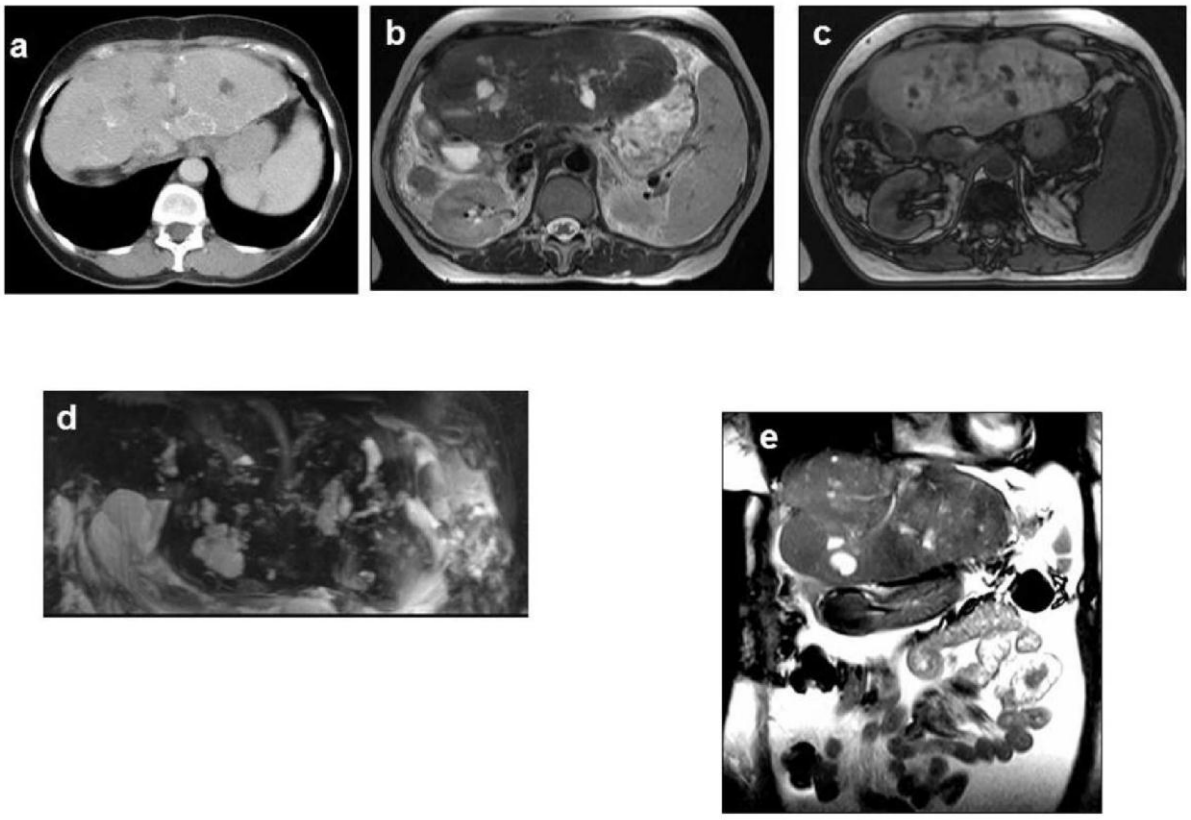

Fig. 7: Post-chemoembolization cholangiopathy with secondary biliary cirrhosis and ascites. 60 years old female cholangiocarcinoma patient underwent TACE for liver remnant multiple recurrent tumors. CT (a), MRI T1-WI (b), T2-WI(c) and MRCP (d) shows multiple strictures and postnecrotic cysts of bile ducts, non-neoplastic nodularity of the liver with evidence of ascites at coronary T2-WI (e).

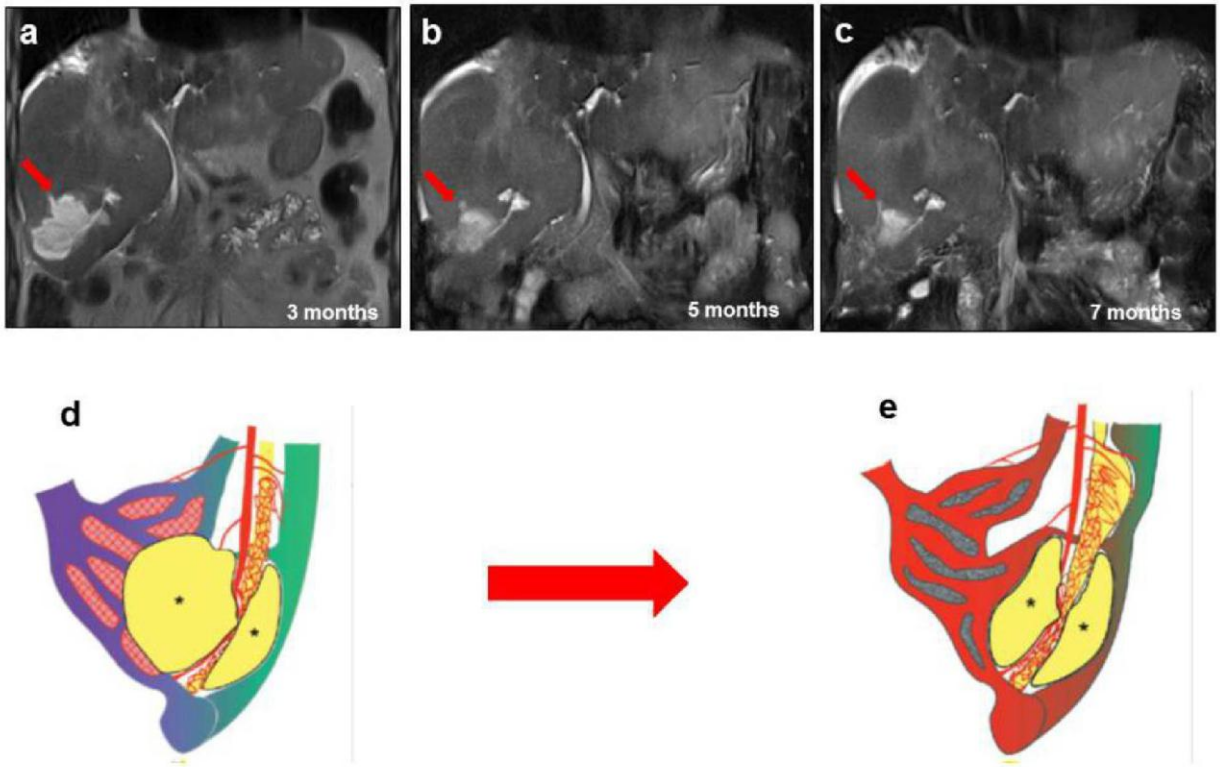

Fig. 8: MRI and schemata of acute and chronic TACE-induced bile duct injury. In the acute stage(a,d), necrosis of the bile duct induces rupture of the bile duct and biloma formation (arrow-a,b,c,asterisks-d,e) along the portal tract. A large cystic biloma can occupy the space of the acutely infarcted parenchyma. In the chronic stage, the portal tract injury with stricture and dilatation of the bile ducts is accompanied by gradual portal vein obliteration, resulting in parenchymal atrophy (b,c,e). Schemata from Chung J.et al. Haemodynamic events and localised parenchymal changes following transcatheter arterial chemoembolisation for hepatic malignancy: interpretation of imaging findings // Br J Radiol. 2010 Jan;83(985):71-81)

Conclusion

TACE is gaining growing popularity in the management of the hepatic malignancies due to its wider indications comparing with surgery and ablative therapies, acceptable safety/efficiency profile and possibility of repeated procedures if necessary. Rare severe problems are nevertheless possible. Interventional radiologists are to be aware of post-TACE biliary complications for planning TACE material, inter-TACE intervals and post-procedural therapy.

References

1. Kato T, Nemoto R, Mori H, Takahashi M, Harada M. Arterial chemoembolization with mitomycin C microcapsules in the treatment of primary or secondary carcinoma of the kidney, liver, bone and intrapelvic organs // Cancer. 1981 Aug 1;48(3):674-80.

2. Chung J, Yu JS, Chung JJ, Kim JH, Kim KW. Haemodynamic events and localised parenchymal changes following transcatheter arterial chemoembolisation for hepatic malignancy: interpretation of imaging findings // Br J Radiol. 2010 Jan;83(985):71-81

3. Bhagat N, Reyes DK, Lin M, Kamel I, Pawlik TM, Frangakis C, Geschwind JF. Phase II Study of Chemoembolization With Drug-Eluting Beads in Patients With Hepatic Neuroendocrine Metastases: High Incidence of Biliary Injury // Cardiovasc Intervent Radiol. 2012 Jun 22. [Epub ahead of print]

4. Guiu B, Deschamps F, Aho S, Munck F, Dromain C, Boige V, Malka D, Leboulleux S, Ducreux M, Schlumberger M, Baudin E, de Baere T. Liver/biliary injuries following chemoembolisation of endocrine tumours and hepatocellular carcinoma: lipiodol vs. drug-eluting beads //J Hepatol. 2012 Mar;56(3):609-17.

Personal Information

ПОСТЕР

Perspective approaches in the evaluation of the preoperative chemotherapy of bone sarcomas using plain radiography.

Poster No.:	C-0333
Congress:	ECR 2013
Type:	Scientific Exhibit
Authors:	A. Bludov, Y. Zamogilnaya, N. Kochergina, A. Nered; Moscow/RU
Keywords:	Education and training, Cancer, Diagnostic procedure, Decision analysis, Chemotherapy, CAD, Plain radiographic studies, Oncology, Musculoskeletal system, Musculoskeletal bone
DOI:	10.1594/ecr2013/C-0333

Purpose

Bone sarcomas represent approximately 1% of malignant neoplasms in adults. Although advances in chemotherapy and surgery have improved prognosis, sarcomas still are fatal in up to half of patients. Histologic response has been shown to be a "gold standard" in the evaluation of neoadjuvant chemotherapy, it is considered to be the main prognostic factor and the criterion defining the postoperative treatment. Due to the Huvos Tumor Necrosis Grading System based upon the percentage of post-treatment necrosis bone sarcomas are categorized as showing good (# 90% of necrosis) or poor (# 90% of necrosis) responses. To avoid the patient to continue on ineffective chemotherapy protocol there is a need in imaging method which reliably determines success or failure of preoperative chemotherapy prior to surgery and pathologic analysis of tumor.

Plain radiography is the first imaging method which was used to assess the effectiveness of preoperative chemotherapy in bone sarcomas. Review of the literature shows a wide range of sensitivity (from 50 to 91%) and specificity (from 33 to 87%) of plain radiography.

The purposes of our study were:

1. To clarify the radiographic signs in assessment of the preoperative chemotherapy of bone sarcomas.
2. To develop diagnostic and differential criteria (decisive rule) of poor and good response to the neoadjuvant treatment.
3. To compare the informativeness of developed criteria in the middle and after preoperative chemotherapy.

Methods and Materials

Case selection

To develop and verify the decisive rule for plain radiography we analyzed radiograms of 109 patients with bone sarcomas confirmed by biopsies. 91 patients (83.5%) with osteosarcoma, 9 patients (8.3%) with Ewing sarcoma/PNET, 4 patients (3.7%) with malignant fibrous histiocytoma, 1 patient with mesenchymal chondrosarcoma (0.9%) and 1 patient with round-cell liposarcoma (0.9%). All the patients were treated with systemic neoadjuvant chemotherapy (without preoperative radiotherapy) and primary surgical excision at our institution with post-treatment histological analysis of response.

Chemotherapy and Surgical Technique

Depending on the histological type of the tumor all patients received from four to six cycles of neoadjuvant chemotherapy. 108 patients (99%) underwent limb-sparing surgery with wide resection of the tumor. Only 1 patient was treated with amputation.

Pathology

Gross

The specimens were dissected in the conventional manner. Following measurement, the tumors were serially transected. We fully analyzed one section of the tumor's greatest dimension which was divided into separate segments. In each segment estimation of percent necrosis and residual tumor was recorded. Final histologic response was determined as the sum of the results in all of the segments. Additionally multiple sections were taken from different parts of the tumor as well as from the margins.

Histologic Grading of Response

The tumors were systematically evaluated with a semiquantitative Huvos Tumor Necrosis Grading System. In every case, we determined the percent areas of viable tumor, necrotic tumor, fibrous/hyalinized stroma and acellular tumor osteoid such that the sum of these components was equal to 100%. Based upon the results, the tumors were categorized as having a good response (Grade III-IV) when # 90% of necrosis was present and a poor response (Grade I-II) for # 90% of necrosis Fig. 1 on page 4.

Imaging studies

The patients were examined on three diagnostic stages: before, in the middle and at the end of the course of the preoperative chemotherapy (before surgery). Plain radiography was obtained in the middle and after preoperative chemotherapy at different time periods. 61 patients (56%) were examined both in the middle of chemotherapy and before surgery. 48 patients were examined only on two stages: before and in the middle of the chemotherapy - 16 patients, and before and at the end of the therapy - 32 patients.

Statistics, multifactor analysis and decisive rule

The statistical analysis of the radiographic symptoms was made by STATISTICA program (v. 7.0, Statsoft Inc.,USA), the calculation of the weighted coefficient of each statistically significant symptom was performed using the software "ASTA" invented at the N.N.Blokhin Cancer Research Center (Moscow). "ASTA" besides different statistical programs uses probabilistic mathematical techniques based on Bayes' theorem. In multifactor analysis, statistically significant signs acquire weight coefficients, which determine the frequency of occurrence of these symptoms in a group of patients with good and poor response. Subsequently, on the basis of weight coefficient of each radiographic

symptom the decisive rule was created for both groups of patients, with good and poor response.

For making the decisive rule in our study we used the data of 61 patients which were examined on every three diagnostic stages (before, in the middle and at the end of the preoperative chemotherapy). The decisive rule was checked on two groups. The first one ("middle-stage" group) consisted of the data of 77 studies of the patients examined in the middle of the treatment (16 patients who were examined before and in the middle of the therapy + 61 patients who were examined on three diagnostic stages). The second group ("end-stage" group) consisted of the data of 93 studies of the patients examined at the end of the treatment (32 patients who were examined before and after the therapy + 61 patients who were examined on three diagnostic stages).

Images for this section:

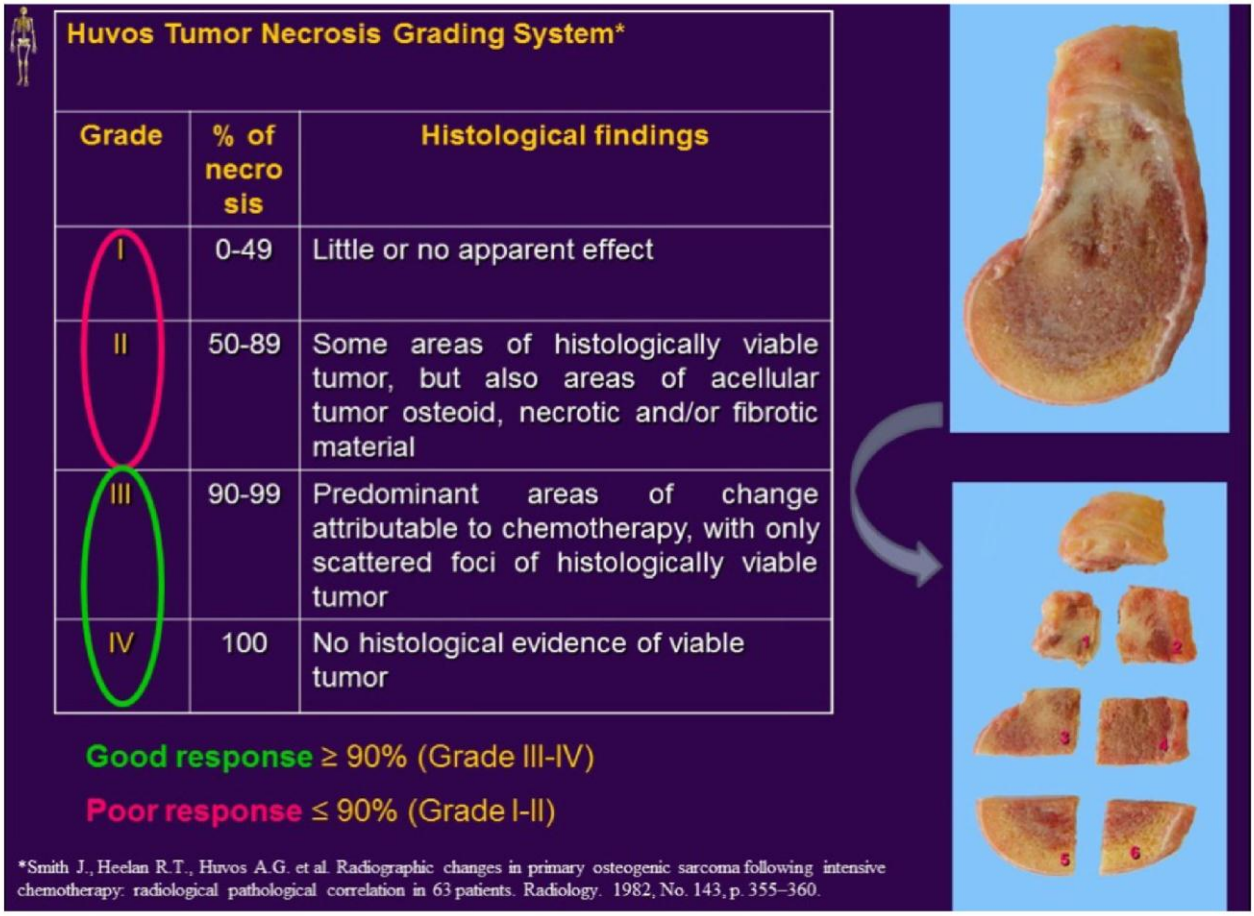

Fig. 1: Huvos Tumor Necrosis Grading System (Smith J., Heelan R.T., Huvos A.G. et al. Radiographic changes in primary osteogenic sarcoma following intensive chemotherapy: radiological pathological correlation in 63 patients. Radiology. 1982, No. 143, p. 355-360)

Results

Developed decisive rule with weight coefficients of radiographic symptoms of the bone tumors during neoadjuvant chemotherapy is illustrated in Table 1.

Table 1. Decisive rule with weight coefficients of radiographic symptoms of the tumor during neoadjuvant chemotherapy.

#	Radiographic signs	Weight coefficient	Radiographic signs	Weight coefficient
1	No increasing of plastic component	-24	Increasing of plastic component	+27
2	No increasing of lytic component	-7	Increasing of lytic component	+59
3	Presence/ extension of peripheral sclerotic rim in the bone	-98	Absence of peripheral sclerotic rim in the bone	+13
4	Enlarged surrounding soft tissue mass remains without any dynamic	-21	Increasing of the enlarged surrounding soft tissue mass	+230
5	Decreasing of enlarged surrounding soft tissue mass	-41	Absence of foci with the structure of trabecular bone in the tumor	+3
6	Appearance/ enlargement of foci with the structure of trabecular bone in the tumor or most of	-40	Absence of foci with cellular-trabecular structure in the tumor	+7

	the tumor transforms into trabecular bone			
8	Appearance/ enlargement of foci with cellular-trabecular structure in the tumor	-69	No reparation of the cortex	+12
9	The whole tumor appears cellular-trabecular	-179	Further destruction of the cortex	+208
10	No change of the cortex	-2	No assimilation of periosteal reaction	+46
11	Partly reparation of the cortex	-101	Non-assimilated periosteal reaction remains without any dynamic	+69
12	Complete assimilation of periosteal reaction	-78	Partial assimilation of periosteal reaction	+17
13	Presence of complete periosteal "shell" enclosing the periphery of the extra-osseous component	-69	Appearance or extension of the new non-assimilated periosteal reaction	+138
14	Increasing of the extension of the periosteal "shell" enclosing the	-56	Presence of the partial periosteal "shell" on the periphery of	+110

	extra-osseous component		the extra-osseous component
15	Partlial consolidation of the pathologic fracture	-101	
16	Complete consolidation of the pathologic fracture	-69	

By marking the radiographic signs in the table and summarizing the coefficients we can make the decision of the result of the chemotherapy. The sum of weight coefficients of radiographic symptoms with "+" value is categorized as having a poor response, on the other hand the sum with "-" value is showing a good response to chemotherapy. Threshold 0.

As we can see from Table 1 on the radiograms of good responders the following signs can be seen:

- presence/extension of peripheral sclerotic rim in the bone
- decreasing of enlarged surrounding soft tissue mass
- appearance/enlargement of foci with the structure of trabecular bone in the tumor or the most of the tumor transforms into trabecular bone
- appearance/enlargement of foci with cellular-trabecular structure in the tumor or the whole tumor appears cellular-trabecular
- partial reparation of the cortex
- complete assimilation of periosteal reaction
- increasing of the extension or presence of complete periosteal "shell" enclosing the extra-osseous component
- partial/complete consolidation of the pathologic fracture

An example of good response is shown on Fig. 2 on page 9 .

Radiological signs associated with poor response according to decisive rule are:

- increasing of lytic component
- increasing of the enlarged surrounding soft tissue mass
- further destruction of the cortex
- no assimilation of periosteal reaction or non-assimilated periosteal reaction remains without any dynamic
- appearance or extension of the new non-assimilated periosteal reaction

- presence of the partial periosteal "shell" on the periphery of the extra-osseous component

An example of poor response is shown on Fig. 3 on page 10.

Basing on the data in Table 1 the sensitivity (probability of good response) and specificity (probability of poor response) of plain radiography in the middle and at the end of preoperative treatment were calculated and summarized in Table 2. The sensitivity of the plain radiography using the decisive rule on the "middle" diagnostic stage was 81.6%, the specificity was 64.1%. Positive predictive value (PPV) was 78.1 % and negative predictive value (NPV) - 68.9 %. At the end of the preoperative treatment the values of the sensitivity and specificity increased up to 85.4% and 68.9% correspondingly with PPV of 81.6 % and NPV of 74.6%.

Table 2. Significance of plain radiography using decisive rule on the both diagnostic stages

Radiologic response	**Pathologic response**		**Number of examinations**
	Poor (Grade I-II)	**Good (Grade III-IV)**	
"MIDDLE" DIAGNOSTIC STAGE (IN THE MIDDLE OF THE NEOADJUVANT CHEMOTHERAPY)			
Poor response	31	7	38
Good response	14	25	39
Number of examinations	45	32	**77**
SENCITIVITY			81,6%
Confidence interval			(69,3% - 93,9%)
SPECIFICITY			64,1%
Confidence interval			(49,05% - 79,15%)
Positive Predictive Value (PPV)			78,1%
Confidence interval			(63,78% - 92,42%)
Negative Predictive Value (NPV)			68,9%
Confidence interval			(55,4% - 82,4%)
FINAL DIAGNOSTIC STAGE (AT THE END OF THE COURSE OF TREATMENT)			
Poor response	41	7	48

Good response	14	31	45
Number of examinations	55	38	**93**

SENCITIVITY	85,4%
Confidence interval	(75,4% - 95,4%)
SPECIFICITY	68,9%
Confidence interval	(55,4% - 82,4%)
Positive Predictive Value (PPV)	81,6%
Confidence interval	(68,9% - 84,3%)
Negative Predictive Value (NPV)	74,6%
Confidence interval	(63,1% - 86,1%)

Images for this section:

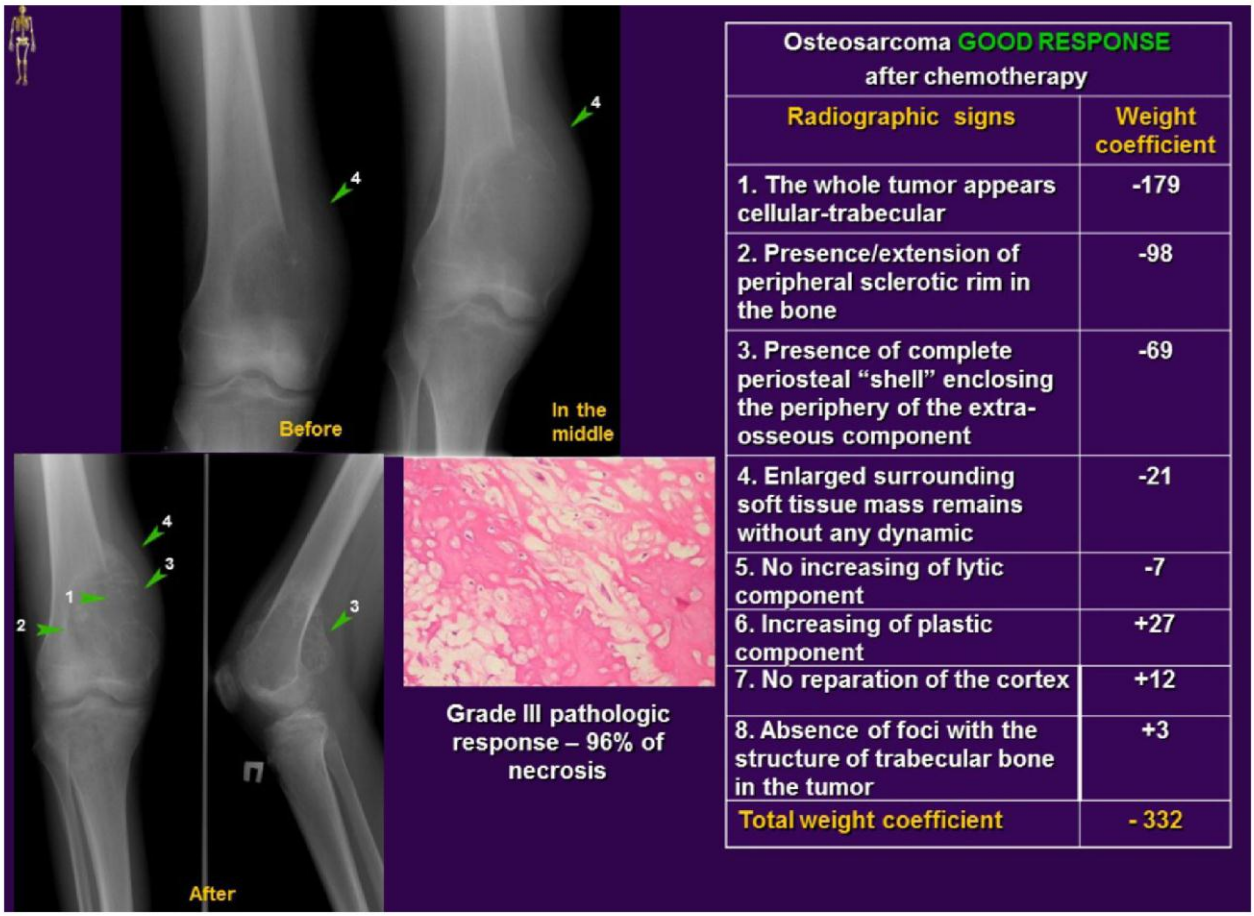

Fig. 2: Radiograms of osteosarcoma of the femur before, in the middle and at the end of the chemotherapy. During the chemotherapy the foci with cellular-trabecular structure and the partial periosteal "shell" appear. Before surgery the "shell" encloses the tumor, which became denser and fully transformed into cellular-trabecular structure. The decisive rule on the final diagnostic stage shows a good response to the treatment (TWC: -322), which was confirmed histologically (Grade III pathologic response).

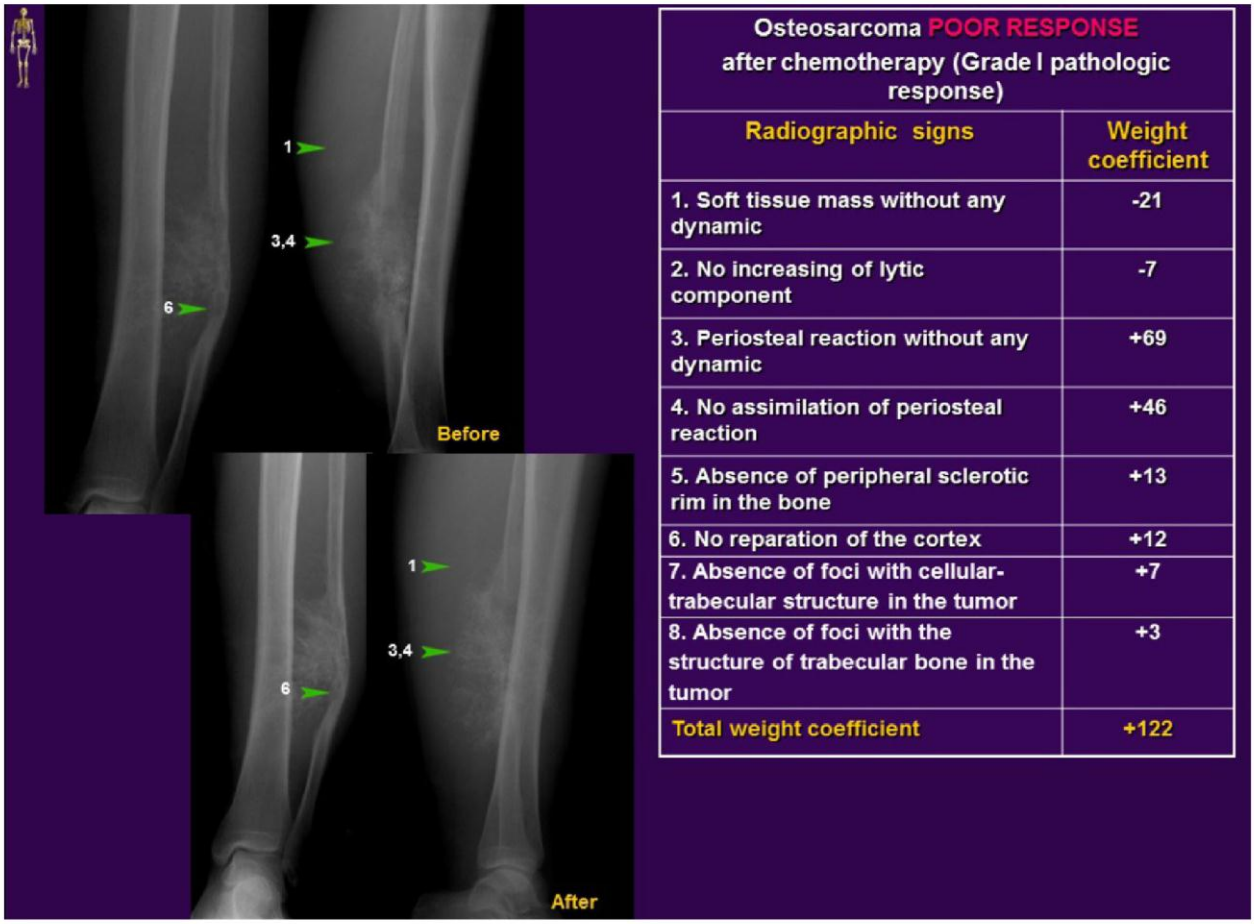

Osteosarcoma POOR RESPONSE after chemotherapy (Grade I pathologic response)	
Radiographic signs	Weight coefficient
1. Soft tissue mass without any dynamic	-21
2. No increasing of lytic component	-7
3. Periosteal reaction without any dynamic	+69
4. No assimilation of periosteal reaction	+46
5. Absence of peripheral sclerotic rim in the bone	+13
6. No reparation of the cortex	+12
7. Absence of foci with cellular-trabecular structure in the tumor	+7
8. Absence of foci with the structure of trabecular bone in the tumor	+3
Total weight coefficient	+122

Fig. 3: Radiograms of osteosarcoma of the fibula before and at the end of the chemotherapy. At the end of chemotherapy the size of the soft tissue mass is the same, the bone and the cortex destruction still persist. The character of periosteal reaction stays the same. Poor response according to decisive rule (TWC: +122), Grade I pathologic response.

Conclusion

Developed diagnostic criteria showed high informativeness of the following radiographic signs in the predilection of good response to chemotherapy (# 90% of necrosis): appearance or enlargement of foci with the cellular-trabecular structure in the tumor, reparation of the cortex, consolidation of the pathologic fracture, and appearance of foci with the structure of trabecular bone in the tumor. For patients with poor response (# 90% of necrosis) typical symptoms are: increasing of enlarged surrounding soft tissue mass, appearance or extension of non-assimilated periosteal reaction or when non-assimilated periosteal reaction remains without any dynamic, further destruction of the cortex and presence of the partial periosteal "shell" on the periphery of the extra-osseous component.

The sensitivity of the plain radiography using the decisive rule on the "middle" stage was 81.6%, the specificity was 64.1%. Positive predictive value (PPV) was 78.1 % and negative predictive value (NPV) - 68.9 %.

At the end of the preoperative treatment the values of the sensitivity and specificity increased up to 85.4% and 68.9% correspondingly with PPV of 81.6 % and NPV 74.6%.

The use of the decisive rule will improve the evaluation of the preoperative chemotherapy of bone sarcomas using plain radiography especially for young radiologists. Moreover these criteria can be used in the educational process.

References

1. Aliev M. The formation and the current state of the domestic oncology orthopedics. Vopr Onkol. 2005; 51(3):283-7.
2. Salzer-Kuntschik M., Delling G., Beron G. et al. Morphological grades of regression in osteosarcoma after polychemotherapy - study COSS 80. J Cancer Res Clin Oncol. 1983; 106 Suppl:21-4.
3. Chuang V.P., Benjamin R., Jaffe N. et al. Radiographic and angiographic changes in osteosarcoma after intraarterial chemotherapy. AJR Am J Roentgenol. 1982; 139(6):1065-9.
4. Smith J., Heelan R.T., Huvos A.G. et al. Radiographic changes in primary osteogenic sarcoma following intensive chemotherapy: radiological pathological correlation in 63 patients. Radiology. 1982; 143(2):355-60.

5. Mail J.T., Cohen M.D., Mirkin L.D. et al. Response of osteosarcoma to preoperative intravenous high dose methotrexate chemotherapy. CT evaluation. AJR Am J Roentgenol. 1985; 144(1):89-93.
6. Holscher H.C., Bloem J.L., Nooy M.A. et al. The value of MR imaging in monitoring the effect of chemotherapy on bone sarcomas. AJR Am J Roentgenol. 1990; 154(4):763-9.
7. Shirkhoda A., Jaffe N., Wallace S. et al. Computed tomography of osteosarcoma after intraarterial chemotherapy. AJR AJR Am J Roentgenol. 1985; 144(1):95-9.
8. Pan G., Raymond A.K., Carrasco C.H. et al. Osteosarcoma: MR imaging after preoperative chemotherapy. Radiology. 1990; 174(2):517-26.
9. Bloem J.L., Reiser M.F., Vanel D. Magnetic resonance contrast agents in the evaluation of the musculoskeletal system. Magn Reson Q. 1990; 6(2):136-63.
10. Erlemann R., Reiser M.F., Peters P.E. et al. Musculoskeletal neoplasms: static and dynamic Gd-DTPA-enhanced MR imaging. Radiology. 1989; 171(3):767-73.
11. Picci P., Bacci G., Campanacci D. et al. Histologic evaluation of necrosis in osteosarcoma induced by chemotherapy: regional mapping of viable and nonviable tumor. Cancer. 1985; 56(7):1515-21.

Personal Information

Alexander Bludov,

Department of Diagnostic and Interventional Radiology, Musculoskeletal Division, N.N. Blokhin Cancer Research Center RAMS, Moscow, Russia.

bludov1982@gmail.com

Yanna Zamogilnaya,

Resident at Department of Diagnostic and Interventional Radiology, Musculoskeletal Division, N.N. Blokhin Cancer Research Center RAMS, Moscow, Russia.

yzamogilnaya@gmail.com

Natalia Kochergina, Prof., Dr.Dr.h.c., M.D., Ph.D.,

Department of Diagnostic and Interventional Radiology, Musculoskeletal Division, N.N. Blokhin Cancer Research Center RAMS, Moscow, Russia.

Anastasia Nered,

Resident at Department of Diagnostic and Interventional Radiology, Musculoskeletal Division, N.N. Blokhin Cancer Research Center RAMS, Moscow, Russia.

ПОСТЕР

Diagnostic efficiency of diffusion-weighted MR imaging in benign liver tumors.

Poster No.:	C-0087
Congress:	ECR 2013
Type:	Scientific Exhibit
Authors:	B. Medvedeva, K. Lukiyanchenko, A. Lukianchenko; Moscow/RU
Keywords:	Liver, MR, Contrast agent-intravenous, Education and training
DOI:	10.1594/ecr2013/C-0087

Purpose

To evaluate the diagnostic efficiency of diffusion-weighted MR imaging in benign liver tumors.

Methods and Materials

25 patients (w/m - 18/7, mean age - 54, range 36-72) with focal liver lesions underwent 1.5 T Gd-EOB-DTPA-enhanced MRI with respiratory-triggered DW EPI (with b-values=50, 400, 800 s/mm2). A total of 57 benign lesions (mean size - 7,75cm, range 0,5-15cm) were evaluated: hepatic adenomas (HA) - 15 lesions, focal nodular hyperplasia (FNH) - 42 lesions. All the lesions were confirmed by well-known typical contrast enhancement MR imaging features and percutaneous biopsy or surgical excision.

Results

On dynamic contrast-enhanced MRI, hepatic adenomas (HA) showed heterogenous hypervascularity during the arterial phase and became slightly hyperintense in the portal venous phase, whereas in the hepatobiliary phase they typically showed contrast agent washout. FNH were usually more vascular than HA and had strong homogenous signal intensity during the arterial phase and became isointense to slightly hyperintense in the portal venous phase. During the hepatobiliary phase FNH typically showed no contrast agent washout. On DW MRI 41 lesions (97,6%) of FHN showed restricted diffusion at low and high b-values, the only one lesion remained isointensive with hypointense central scar. 15 lesions (35,7%) of FNH (in 10 patients) on the ADC maps showed isointensive signal with hyperintense central scar and 27 lesions (64,3%) in 12 patients had isointensive signal. 14 of 15 HA in 4 patients showed no restricted diffusion at low and high b-values and had isointensive to mildly hypointensive signal on the ADC maps. The only one HA was hyperintensive at low and high b-values and remained hypointense on the ADC map.

Images for this section:

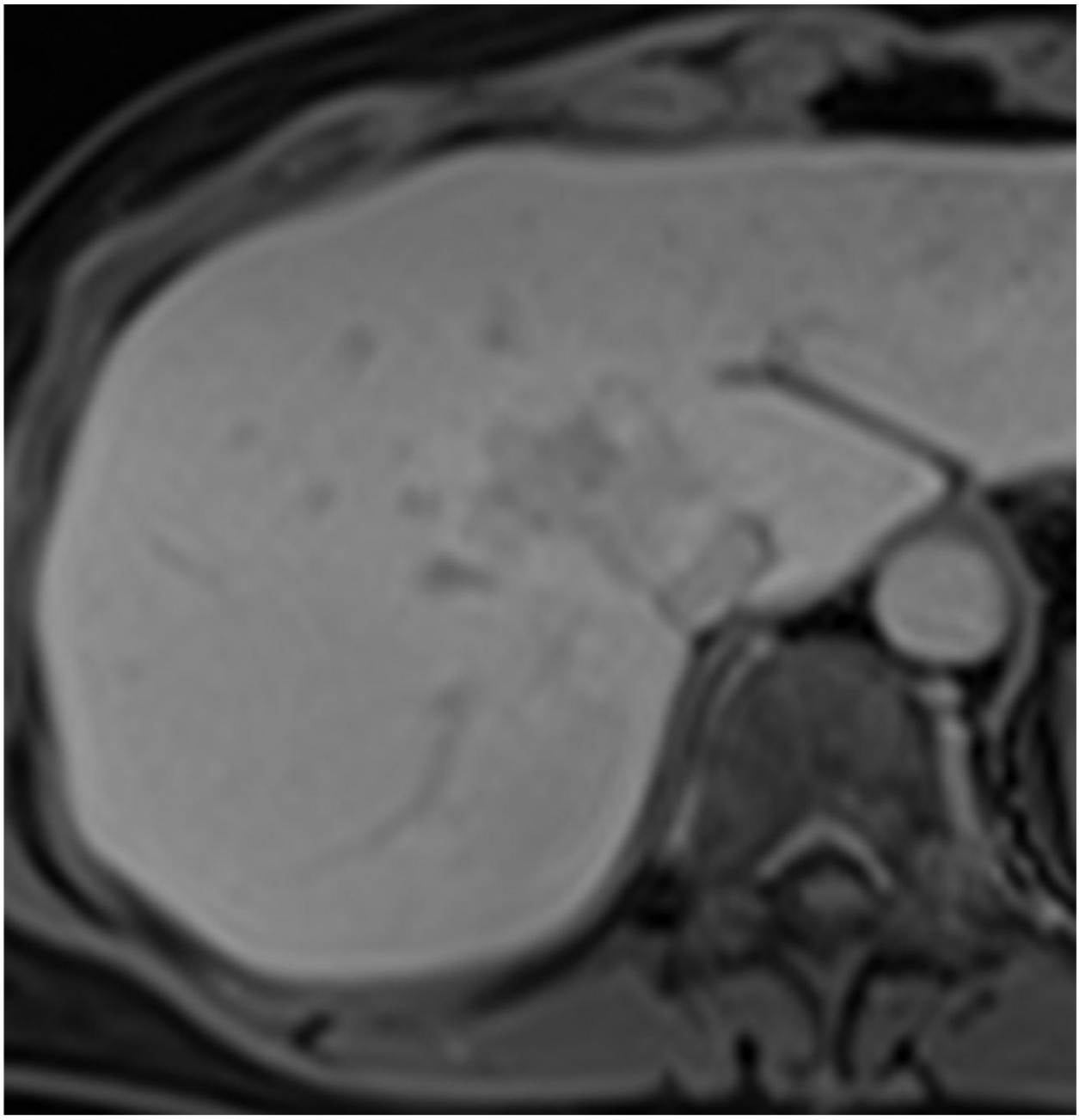

Fig. 1: 50-year-old female patient with FNH. FNH shows no contrast agent washout during the hepatobiliary phase (20 min after injection of Gd-EOB-DTPA) with hypointense central scar.

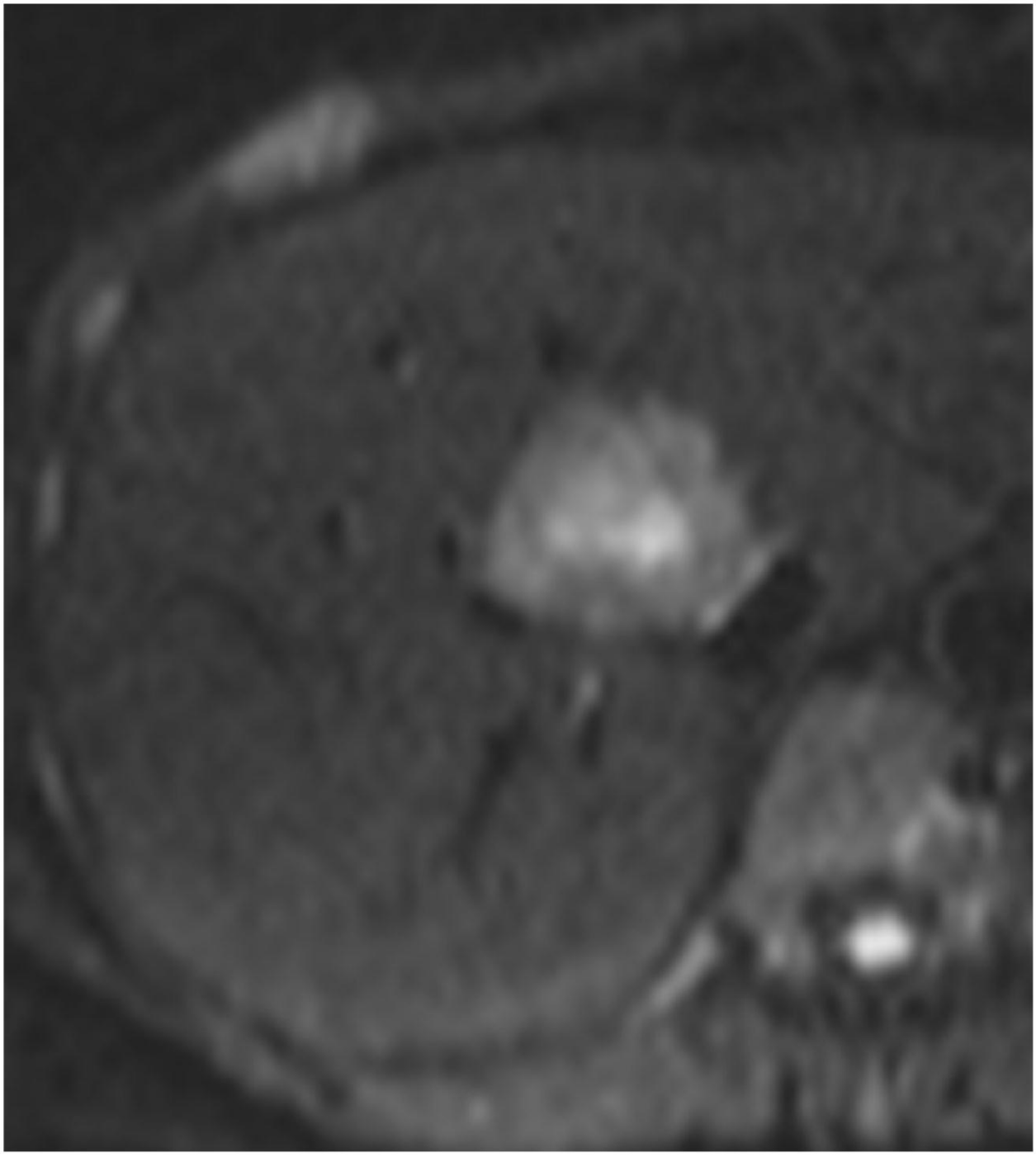

Fig. 2: Diffusion-weighted MRI, b-value=50. The same female patient. FNH shows restricted duffusion.

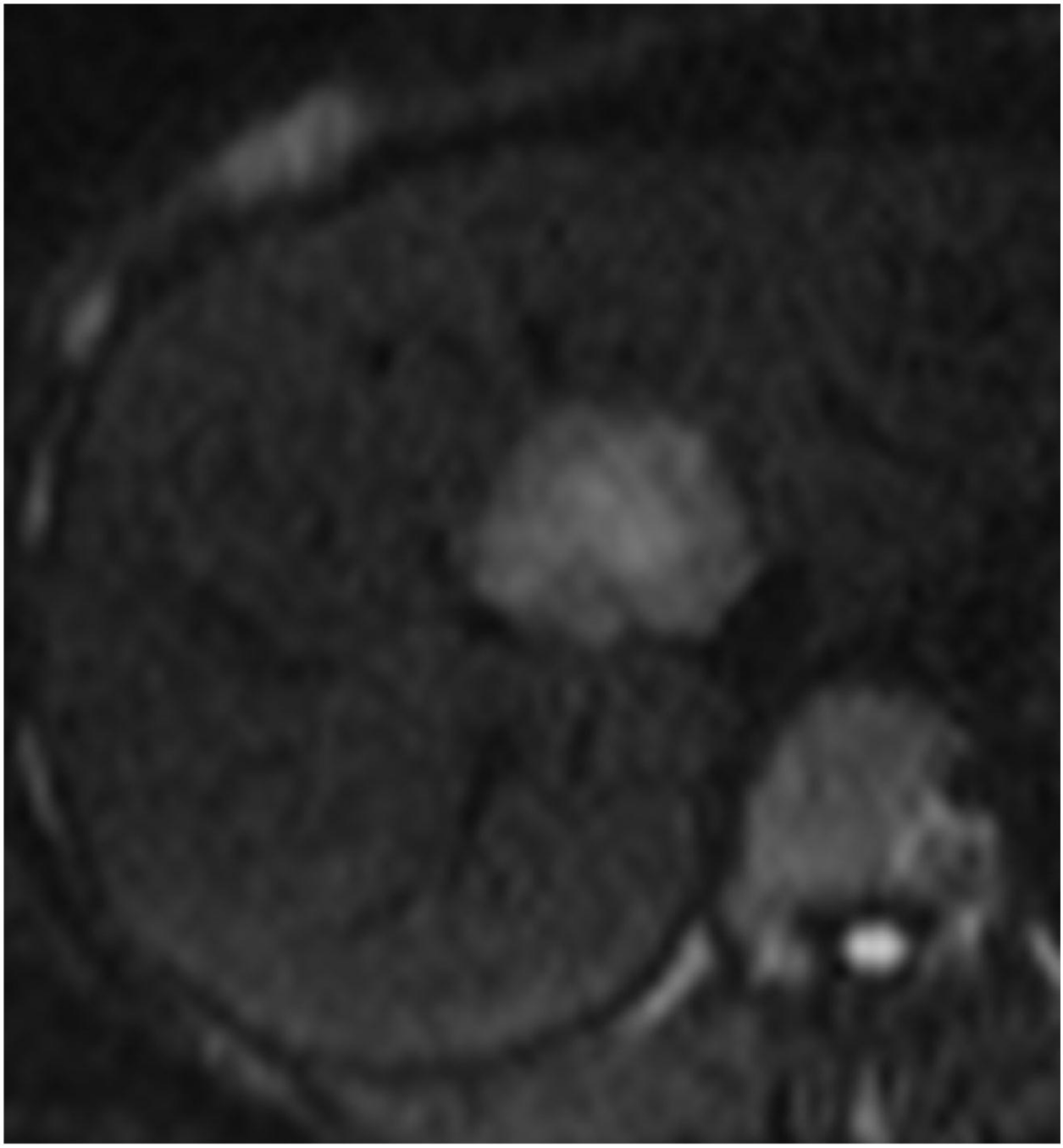

Fig. 3: Diffusion-weighted MRI, b-value=400. FNH shows restricted duffusion.

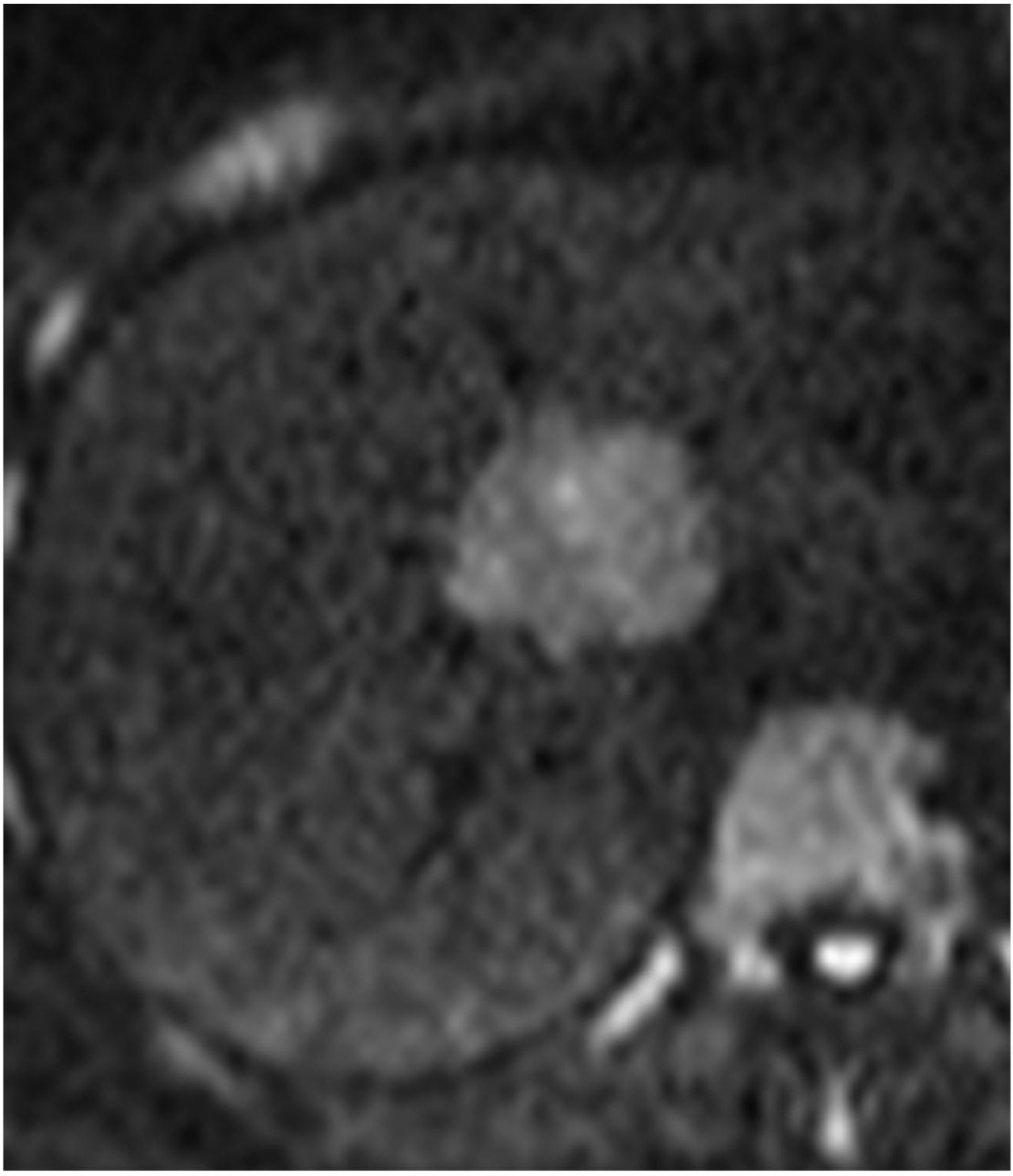

Fig. 4: Diffusion-weighted MRI, b-value=800. FNH shows restricted duffusion.

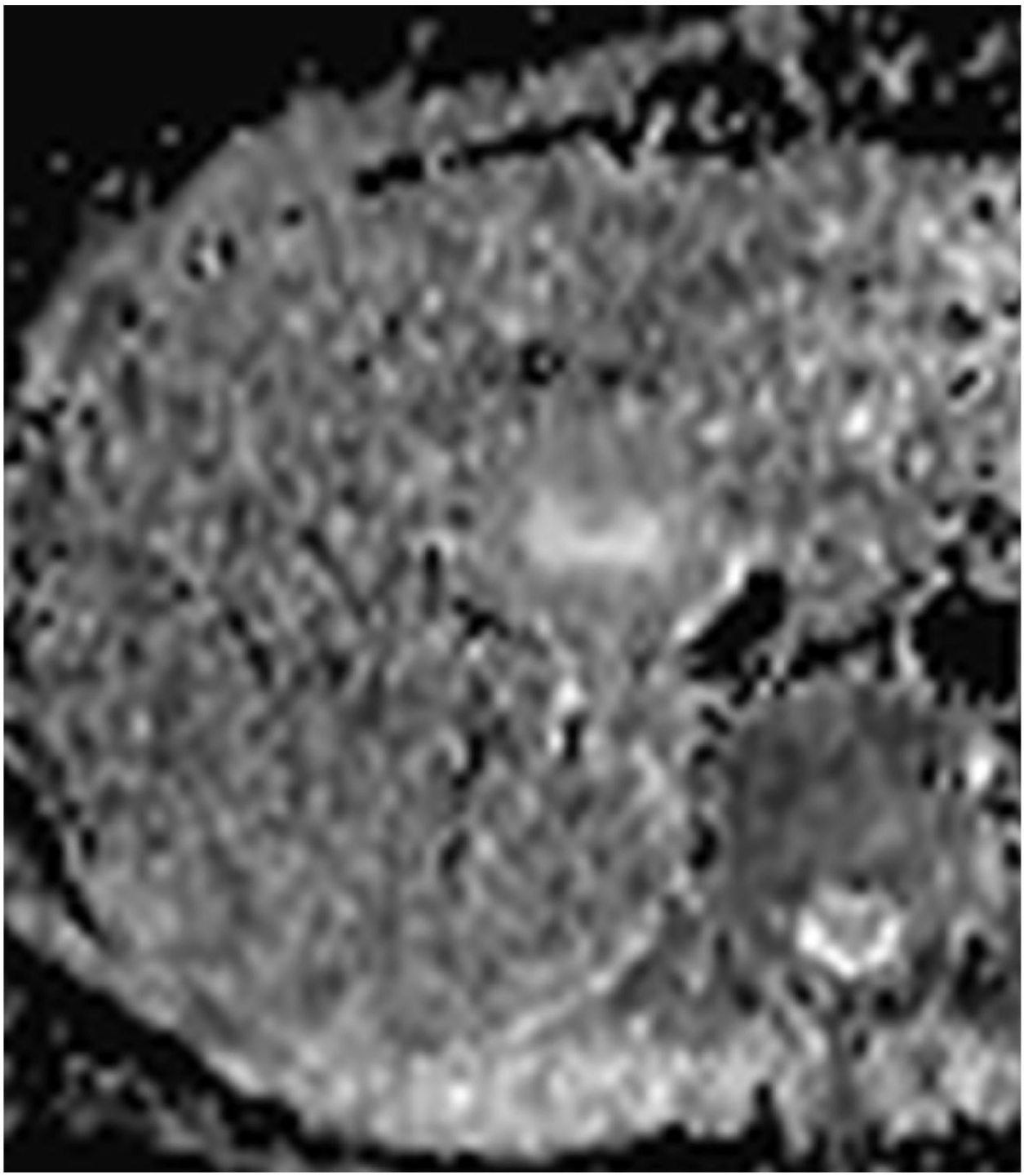

Fig. 5: Diffusion-weighted MRI, ADC map. FNH shows isointensive signal with hyperintense central scar.

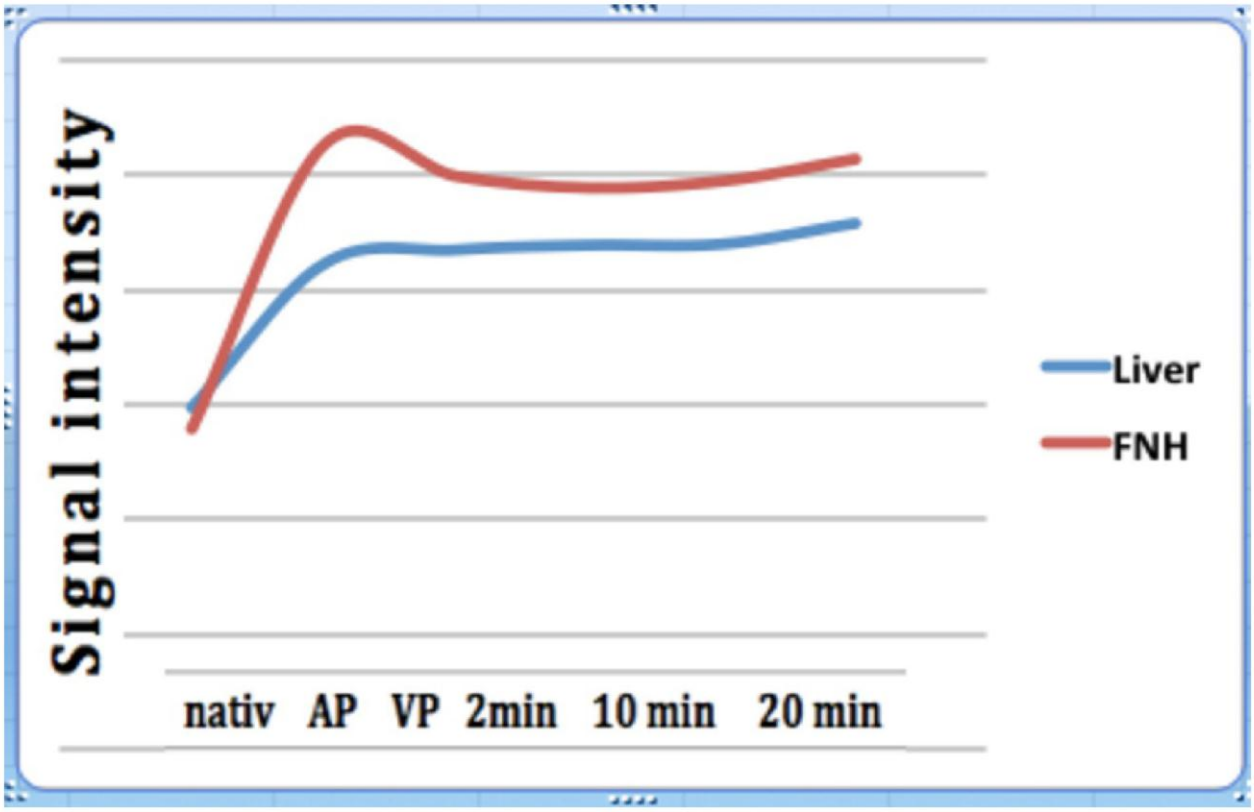

Fig. 6: Signal intensity curve of the liver and FNH during Gd-EOB-DTPA-enhanced MRI.

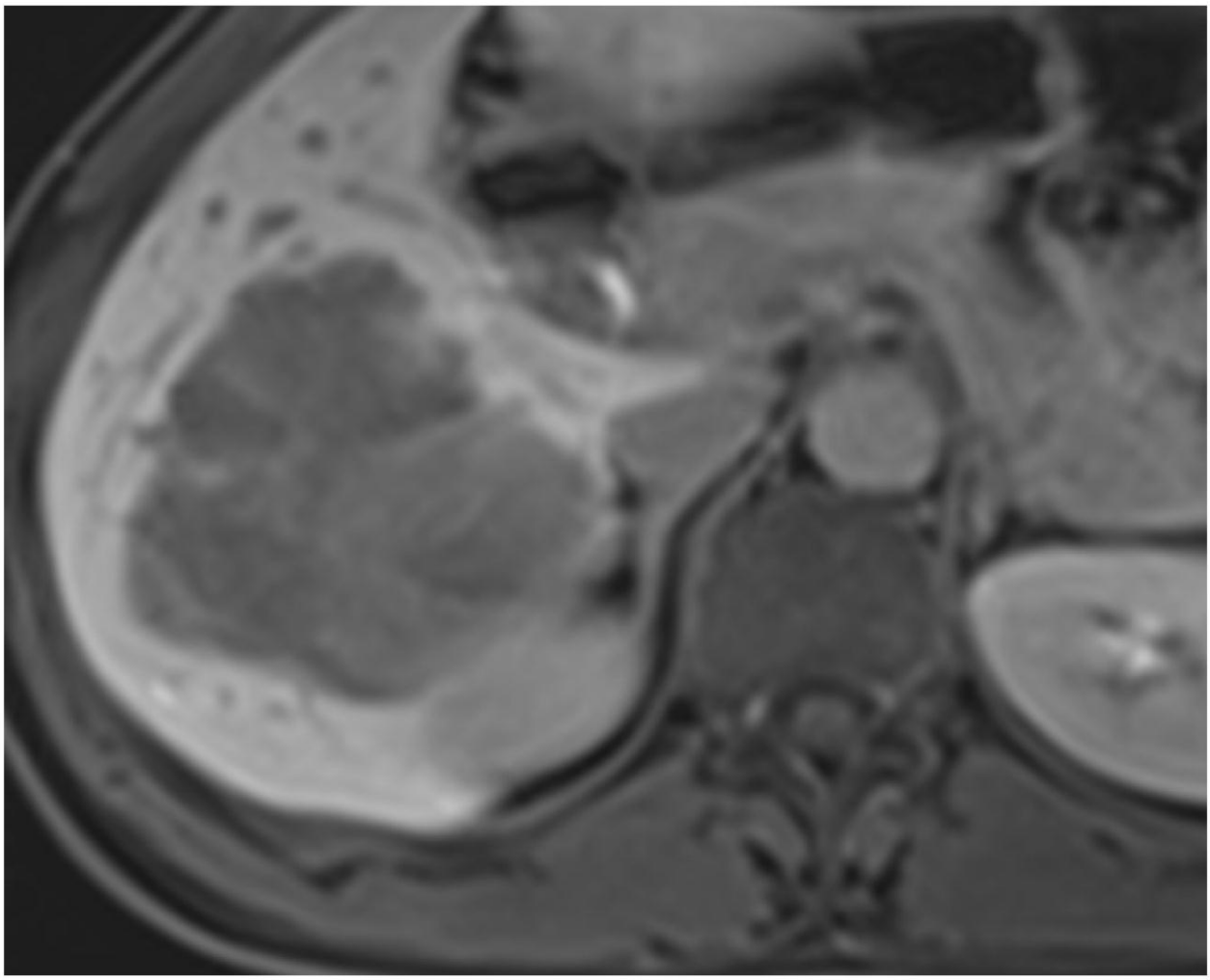

Fig. 7: 47-year-old-female patient with Hepatic Adenoma (HA). HA shows contrast agent washout during the hepatobiliary phase (20 min after injection of Gd-EOB-DTPA)

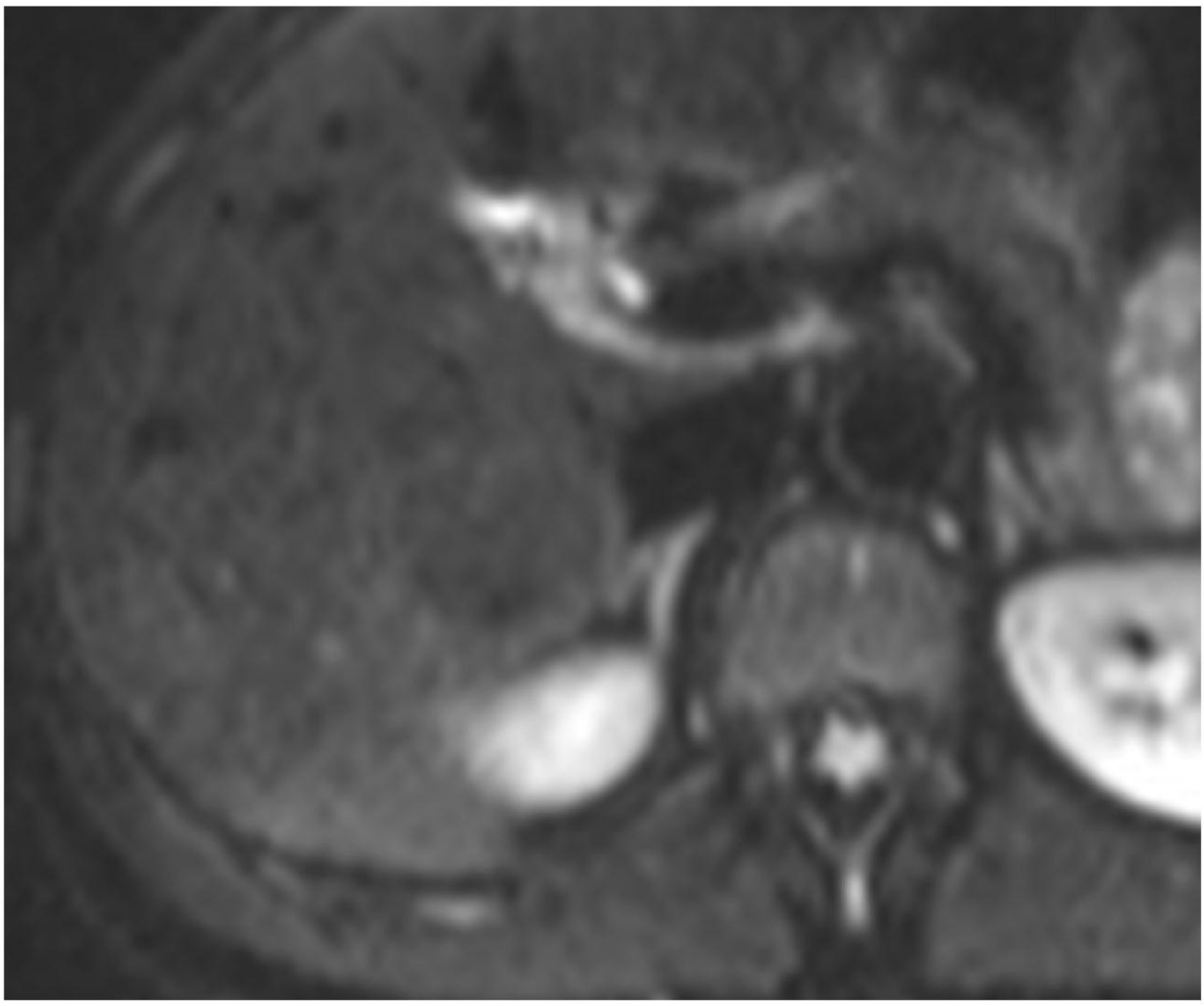

Fig. 8: DW MRI. The same female patient. HA shows no restricted diffusion at b-value=50.

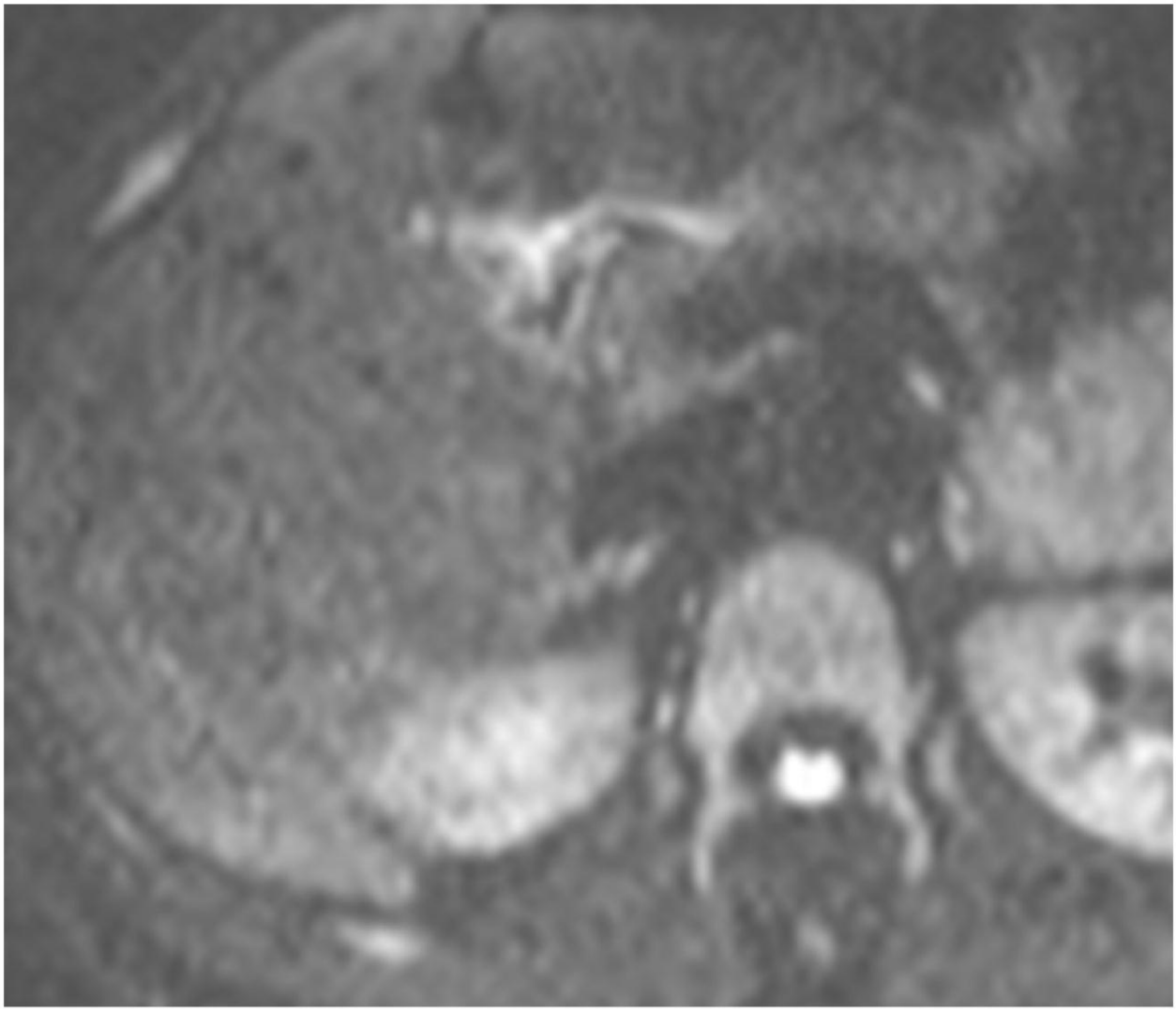

Fig. 9: DW MRI. HA shows no restricted diffusion at b-value=400.

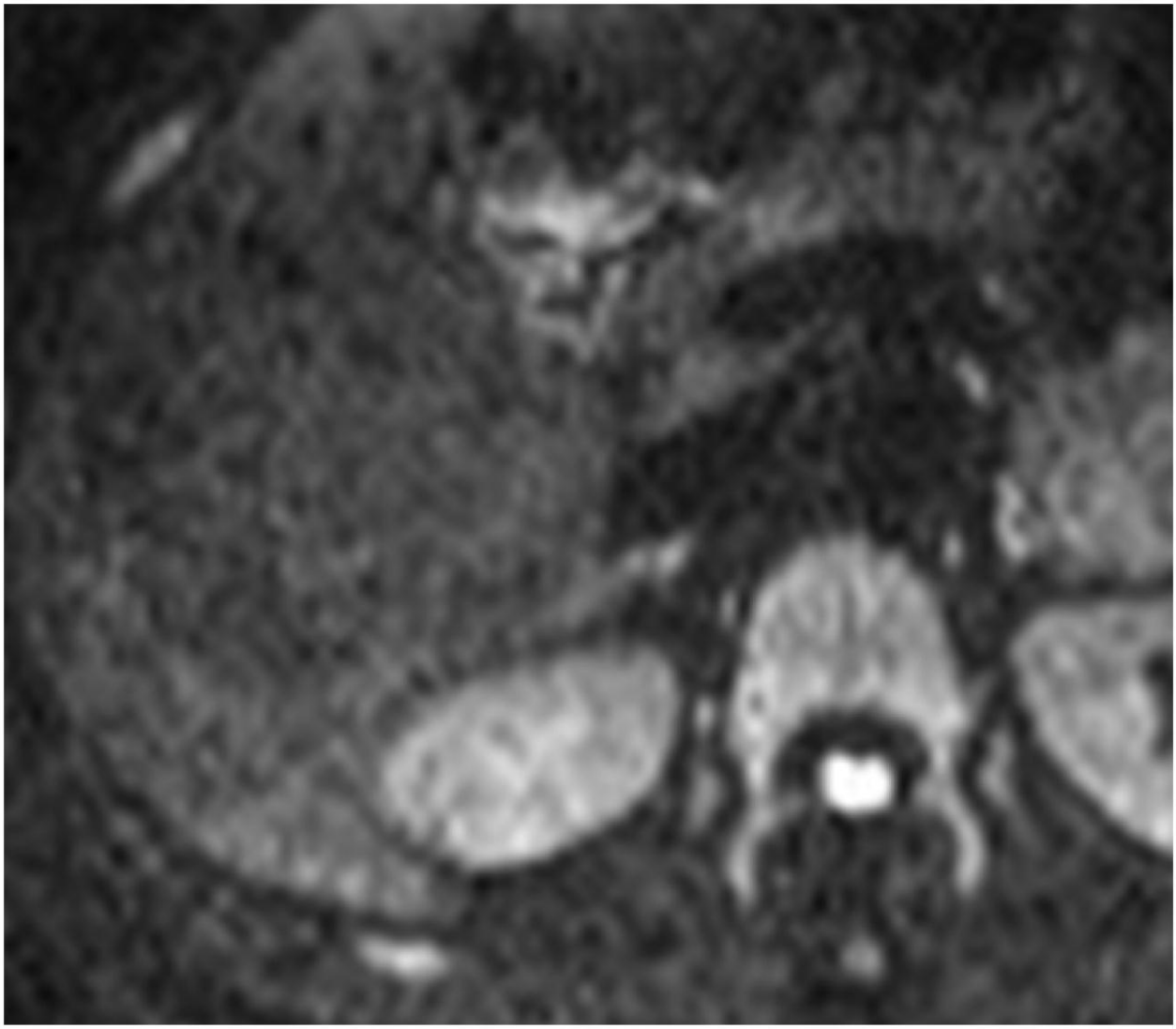

Fig. 10: DW MRI. HA shows no restricted diffusion at b-value=800.

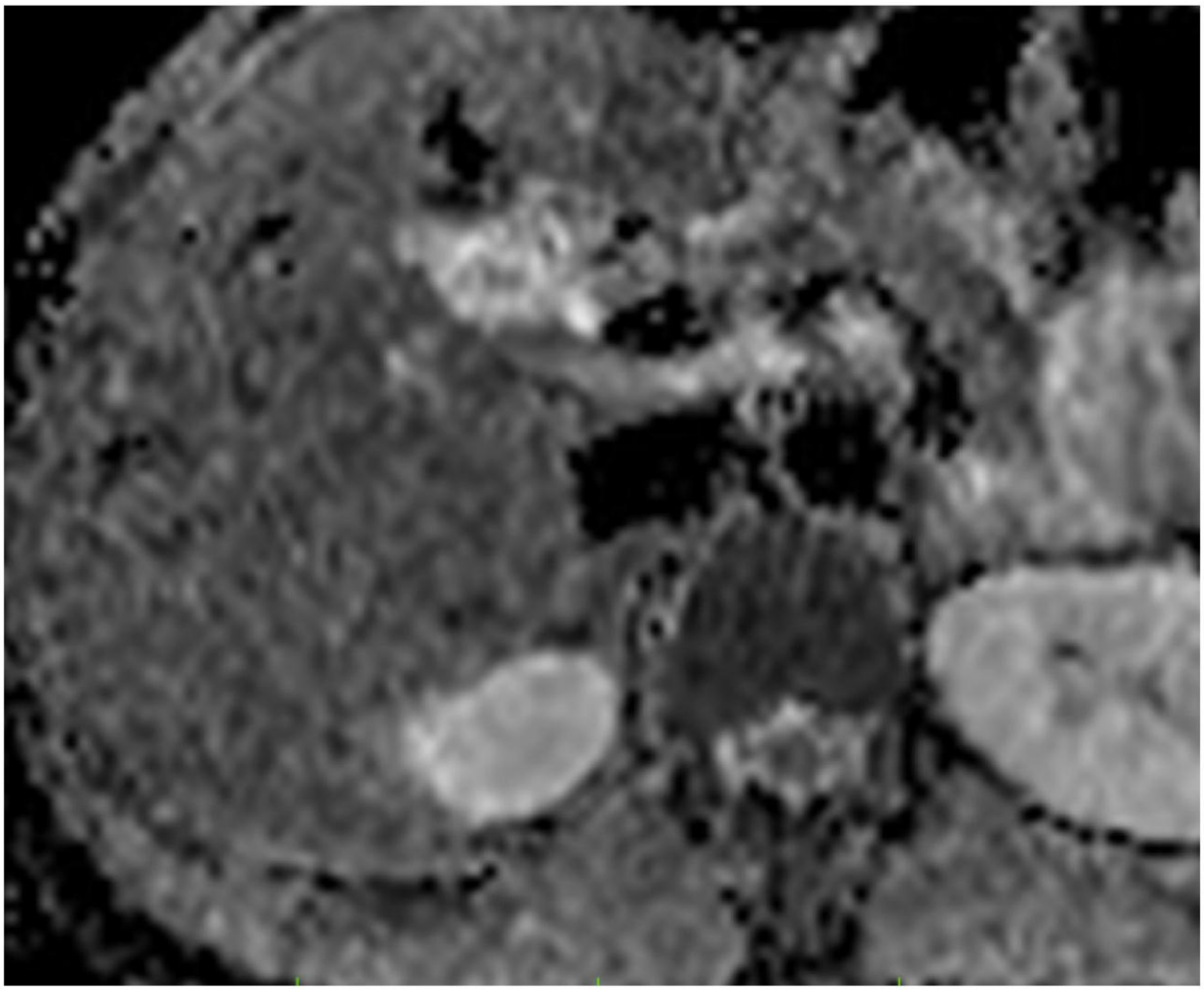

Fig. 11: DW MRI. HA shows isointensive signal at the ADC maps.

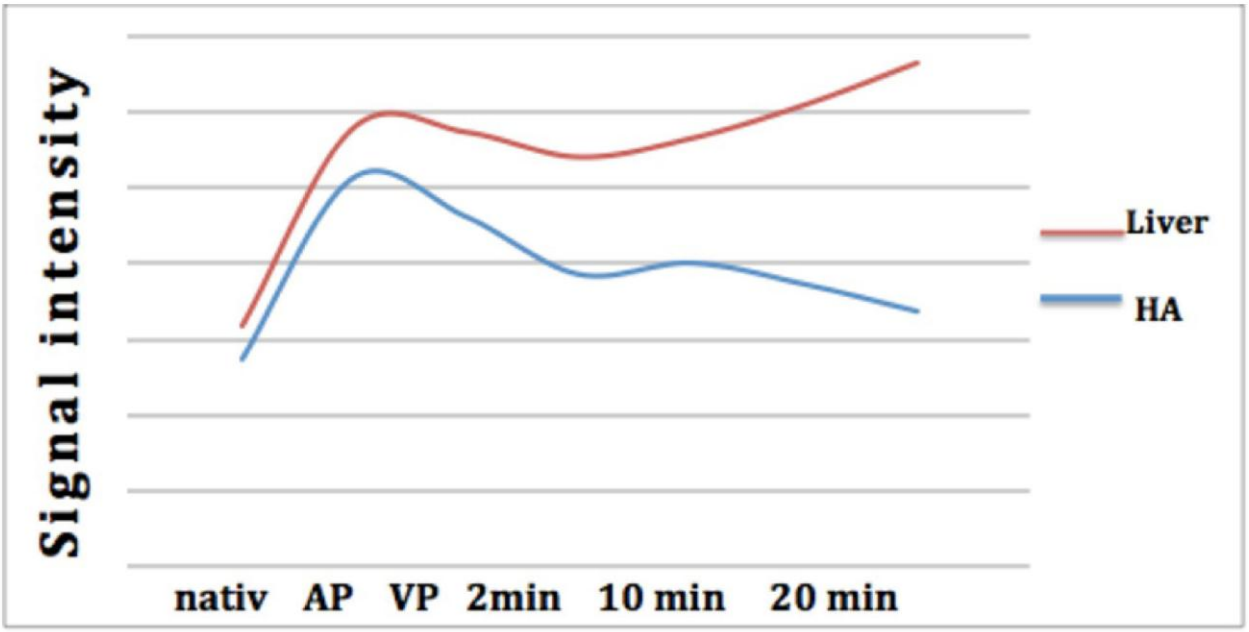

Fig. 12: Signal intensity curve of the liver and HA during Gd-EOB-DTPA-enhanced MRI.

Conclusion

Application of diffusion-weighted MR imaging additionally to contrast-enhanced sequences helps to differentiate some benign focal liver lesions,namely FNH and HA that could prevent unneeded surgery.

References

1. # Tauoli, DM Koh. Diffusion-weighted MR imaging ot the Liver// Radiology: Volume 254: Number 1-Jan 2010.

2.DM Koh, D Collins. Diffusion-weighted MRI in the body: Applications and challenges in Oncology// AJR:188, June 2007

3. Parikh T, et al. Focal liver lesion detection and characterization with diffusion-weighted MR Imaging// Radiology: Volume:246: Number 3-March 2008.

4. A Silva, et al. MR Imaging of hypervascular liver masses: a review of current techniques// RadioGraphics, 2009.

5. Aliya Qayyum. Diffusion-weighted imaging in the abdomen and pelvis:Consepts and applications// RadioGraphics, 2009.

6. XJ Sun, et al. Quantitative evaluation of diffusion-weighted magnetic resonanse imaging of focal hepatic lesions // World J Gastroenterol 2005;11(41):6535-6537.

7. S Feuerlein, et al. Pitfalls in abdominal diffusion-weighted imaging: How predictive is restricted water diffusion for malignancy//AJR:193, 2009.

8. Ichikawa T., et al. Diffusion-weighted MR imaging with a single-shot echoplanar sequence: detection of focal hepatic lesions//AJR, 1998.

9. Braga L., et al. Modern hepatic imaging//Surg Clin North Am. 2004.

10. Motohara T., Semelka RC, et al. MR imaging of benign hepatic tumors//Magn Reson Imaging Clin N Am. 2002.

11. Martin DR, Semelka RC. MR imaging of benign and malignant focal liver lesions// Magn Reson Imaging Clin N Am. 2001.

12. Anderson SW, Kruskal JB, Kane RA. Benign hepatic Tumors and Iatrogenic Pseudotumors// RadioGraphics, 2009.

Personal Information

Ksenia Lukiyanchenko, MD, resident of the Radiology and Imaging department, N.N Blokhin Russian Cancer Research Center/ Moscow.

ПОСТЕР

PHOTODYNAMIC ACTION COMBINED WITH PRO-IMMUNE THERAPEUTICS IN HILAR CHOLANGIOCARCINOMA PATIENTS

O.N. Sergeeva[a*], B.I. Dolgushin[a], V.O. Panov[a], A.V. Kukushkin[a], A.V. Reshetnickov[b]

[a] Russian Academy of Medical Sciences N.N.Blokhin Cancer Research Center. 24, Kashirskoye Shosse, Moscow 115478, Russia, tel. +7 (495) 324 1750, e-mail 7s_olga@mail.ru
[b] RADA-PHARMA International B.V. 82, Westeinde, Noordwijkerhout 2211XR The Netherlands, tel. 0031(71)3642030, e-mail a.reshetnickov@gmail.com .
* To whom correspondence should be addressed.

Intraductal PDT: **results**

Follow up of 15 patients for 1 - 23 months

Alive 7 patients for 1 -19 months. Median of survival 12.5 months

Died 8 patients:

1- in 5 from irrelevant reasons

7 – in 2-23 months after the 1st PDT session from immuno-metabolic disorders

Progression 1 patient

Improving the life quality

All the patients benefited from reducing cholangitis and an anabolic effect since the first intraductal PDT

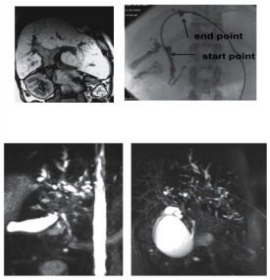

Fifty three PDT procedures (from 1 to 10 per patient) have been performed in 15 biopsy confirmed hilar cholangiocarcinoma patients (5 female, 10 male, age range 40-75y) with previous percutaneous bile duct drainage since February 2008. All the patients had Bismuth IV type tumors and were not surgical candidates. All but 3 patients demonstrated elevated serum bilirubin levels despite of 1 to 4 previous percutaneous transhepatic biliary drainages. The majority of the patients had previously undergone varying therapies or therapy combinations (surgery - 8 patients, radiation therapy chemotherapy – 2 patients, radiation therapy – 1 patient) without success. The median time from the disease onset to the first PDT procedure was 11 months.
The median time of survival after 3-5 PDT procedures was 12 months. All the patients benefited from a better performance status, bile volume increase, decline of serum ALT, AST and total bilirubin levels three weeks after the first intraductal PDT. No a patient showed disease progression. One patient died 5 months after PDT due to non-oncological reasons. Some other patients died due to the wasting syndrome after showing stabilization and even partial responses.
The only patient with intraductal cholangiocarcinoma demonstrated a decrease of intraductal tumor component on MRI. Seven patients are alive from 6 to 19 months without jaundice with absent/minimal wasting.
The longest survival time was 23 months after the 1st PDT.
Sensitizer Radachlorin/Bremachlorin (RADA-PHARMA International B.V., The Netherlands) was used. Radachlorin/Bremachlorin is made of active pharmaceutical substance Radahlorin (5.00g) (total sodium salts of chlorins – 0.35g), water for injections (up to 100.00mL), and additives: N-methyl-D-glucamine (0.20g). It was administered intravenously at the doses of 0.6-2.0mg/kg two to four hours prior to the procedure.
For photoactivation 3W 662±3nm semiconductor laser was employed. At first, a rather aggressive light irradiation with a high fluence rate (340mW/cm^2) and large light dose (approx. 180J/cm^2) was applied, but then we refused from that regimen due to a complicated postprocedural course in the patient. Later we preferred regimens at the pulse mode and low energy fluence rates (40-70mW/cm^2), with light doses of 40-96J/cm^2. Additional immunoadjuvants were used during the latter procedures.

reduction of the tumor intraductal component

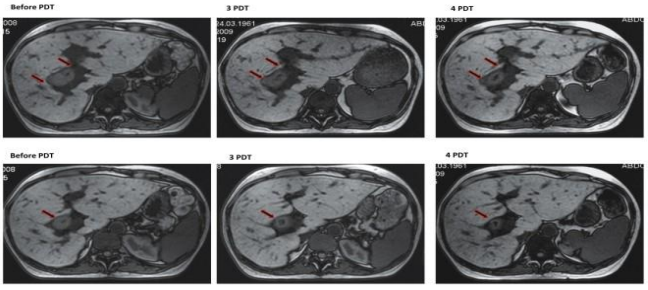

liver remodelling

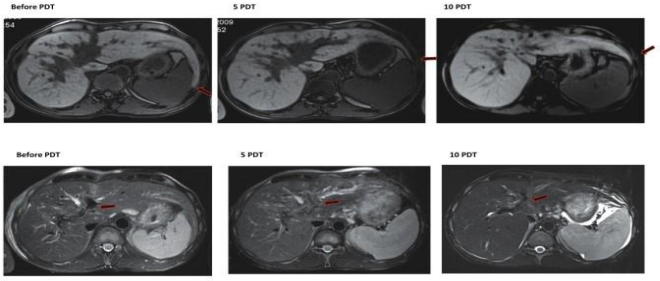

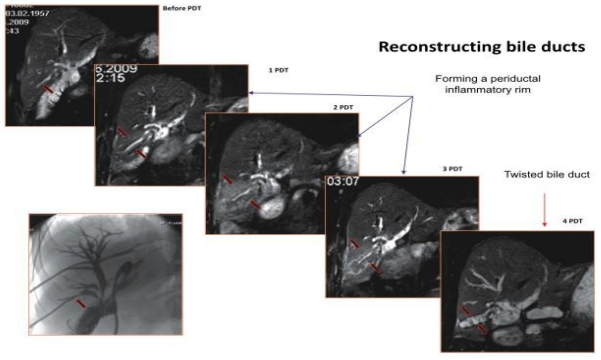

Normalizing the lumen of bile ducts

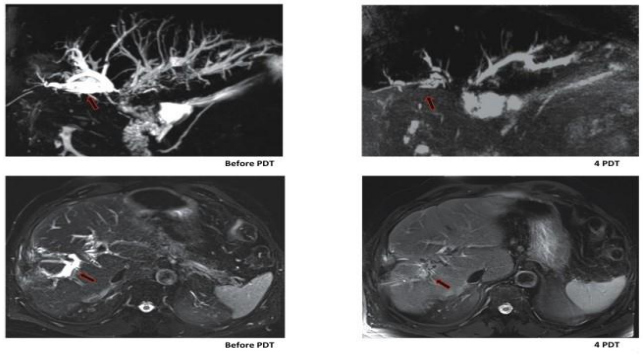

We hypothesize that partial tumor destruction is only a minor PDT action component. PDT also causes some local maturation of tumor-infiltrating myeloid-derived cells (tumor associated macrophages, neutrophil leucocytes, non-matured dendritic cells, etc.) and their specific functioning activation (phagocytosis, movement to the draining lymph nodes, effective antigen presentation and initiation of the specific cytotoxic T-lymphocyte proliferation).

ПОСТЕР

EPOS™ Electronic Presentation Online System

ESR European Society of Radiology

CT perfusion in evaluation of brain metastases vascularity.

Poster No.:	C-0327
Congress:	ECR 2013
Type:	Scientific Exhibit
Authors:	J. Tsibulskaja, A. Lukjanchenko, A. Bekjashev, D. Belov, N. Sevjan, E. Prozorenko, E. Kobjakova, M. Dolgushin; Moscow/RU
Keywords:	Neuroradiology brain, CT, MR-Diffusion/Perfusion, MR, Computer Applications-General, Blood
DOI:	10.1594/ecr2013/C-0327

Purpose

To investigate a role of CT perfusion (PCT) in differential diagnostics of cerebral metastases from various primary sources. CT perfusion allows to differentiate brain tumors with high accuracy, depending on the characteristics of their hemodynamics [1-5]. It is known that metastases and the primary tumor have similar histological and hemodynamic characteristics [5,6]. CT perfusion permits to differentiate metastasis of certain types of tumors and to assume a location of the primary tumor. CT perfusion allows to investigate the physiological characteristics of the affected tissues, but not limited to the assessment of anatomical changes [5,6]. CT perfusion is a not invasive method of exploring hemodynamic characteristics of intracranial tissues in vivo [5,6].

Methods and Materials

We have estimated main CT perfusion parameters in 29 patients with histologically verified metastatic brain lesions.Main bloodparameters - cerebral blood flow (CBF) ml/100g/min, cerebral blood volume (CBV) ml/100g, mean transit time (MTT) sec, permeability of membrane barrier PMB (ml/100ml/min) - have been calculated in different tumor`s parts. We have measured bloodparameters in solid part of tumor (1), nearest tumor perifocal zone (2), vasogenic edema (3), healthy contralateral side (4).

These datasets were acquired on multisection CT scanner Somatom Emotion 6 (a 6-section scanner) (Siemens), time-series of 40 images for 2 slices, thickness 4 mm, time resolution-1s, during the first pass of a 40 ml iodine contrast media bolus intravenously at an injection rate 4 ml/s. The acquisition parameters for PCT studies included 80 kVp and 120 mAs. Dynamic PCT data were processed off line using station Leonardo (Siemens), NeuroVPCT program.

A total of 14 men and 15 women ranging in age from 39 to 75 years were included. Primary tumours located in lung in 11 cases (37.9%), breast - 6 (20.8%), kidney -4 (13.8%), melanoma - 3 (10.3%), colon - 3 (10.3%), gaster - 2 (6.9%).

Results

In solid parts of metastases (zone #1) the highest mean perfusion parameters (CBV (ml/100g/min)/ CBF (ml/100g)/ MTT (sec)/ PMB (ml/100ml/min)) were in renal cancer - 124.06/23.37/7.19/15.71. Mts of melanoma had less rates - 68.24/12.94/7.76/19.74. There was no significant difference between cerebral metastases of lung (42.25/7.18/6.14/18.73) and breast (38.54/7.11/6.23/11.36) cancers.

And the lowest parameters were in cerebral metastases of colon (26.66/4.94/6.46/11.12) and gastric (20.07/4.58/7.11/12.04) cancers.

The mean perfusion parameters in nearest perifocal and edema zones were the lowest in kidney cancer metastases (8.98/2.11/5.17/4.23) because of a tumor capsule.

Images for this section:

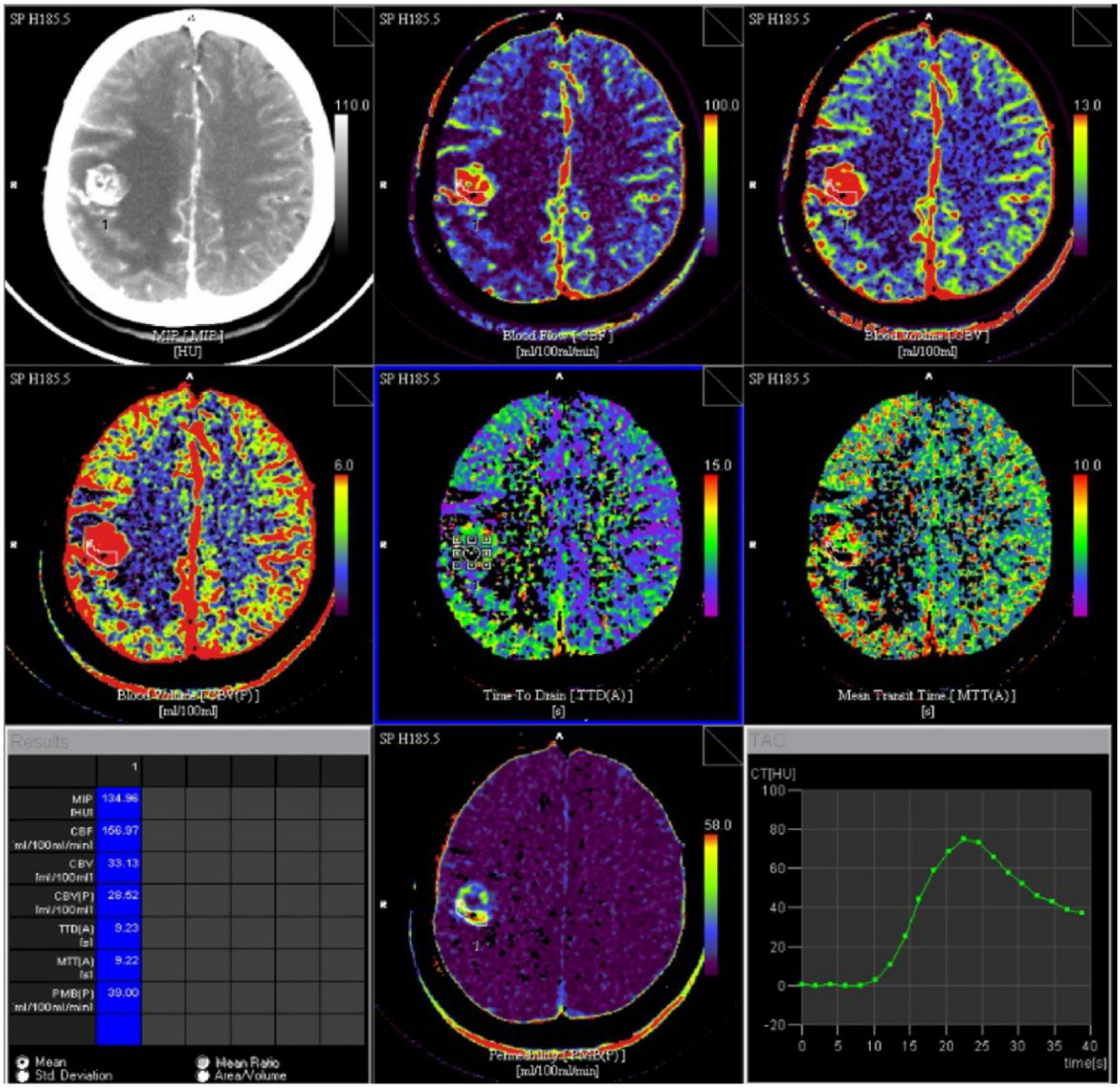

Fig. 1: 61 year old male patient with Mts of renal carcinoma in right parietal area. Histology: renal adenocarcinoma. The highest perfusion parameters were registrated in solid part of tumor: CBF 156.97 ml/100ml/min, CBV 33.13 ml/100ml, MTT 9.22 sec, PMB 39.03 ml/100ml/min. The reason of hyperperfusion was a severity of vascular network.

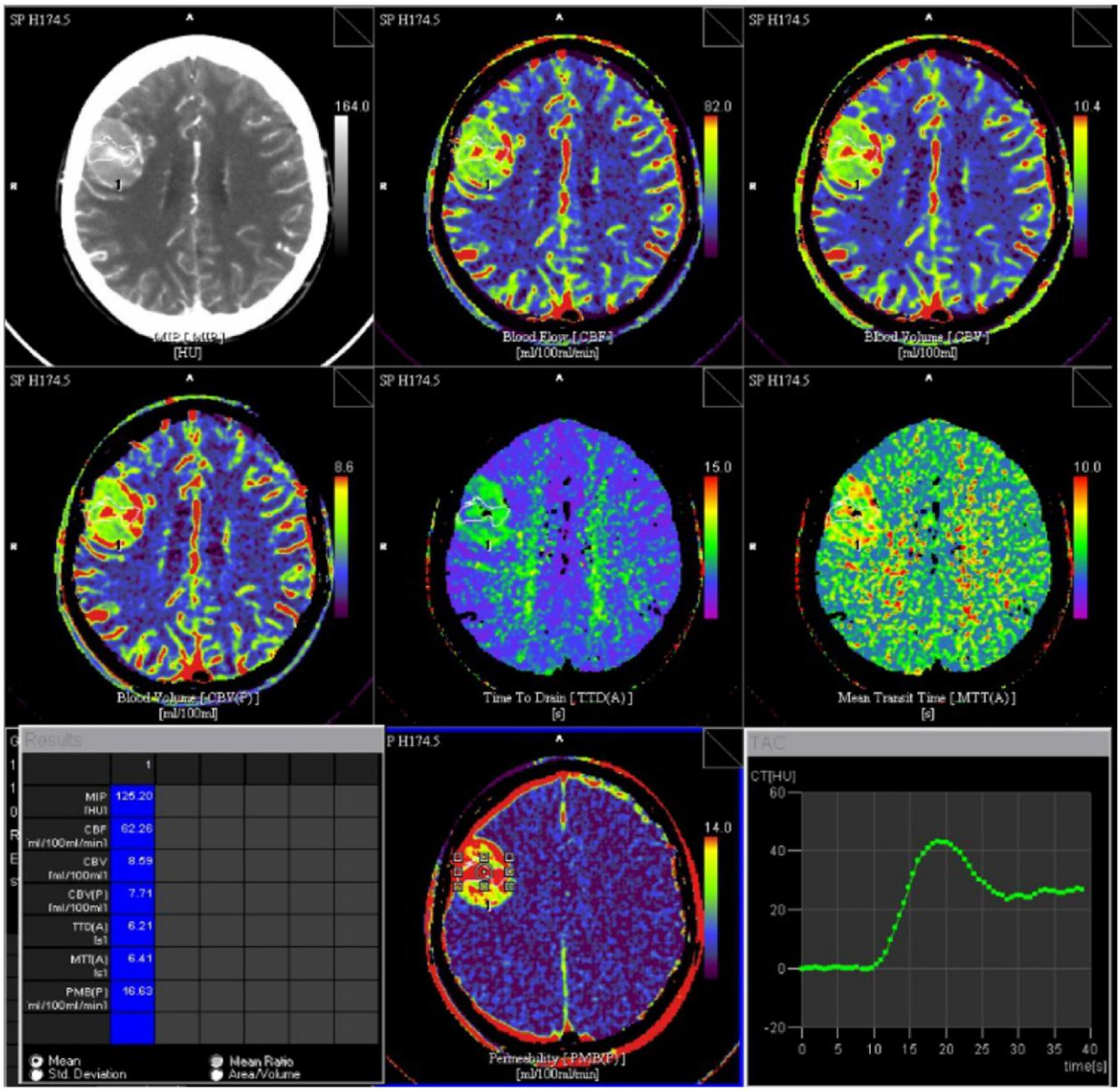

Fig. 2: 46 year old female patient with Mts of melanoma in right frontal area. Histology: pigmental melanoma. Perfusion parameters in solid part were: CBF 62.26 ml/100ml/min, CBV 8.59 ml/100ml, MTT 6.41 sec, PMB 16.63 ml/100ml/min.

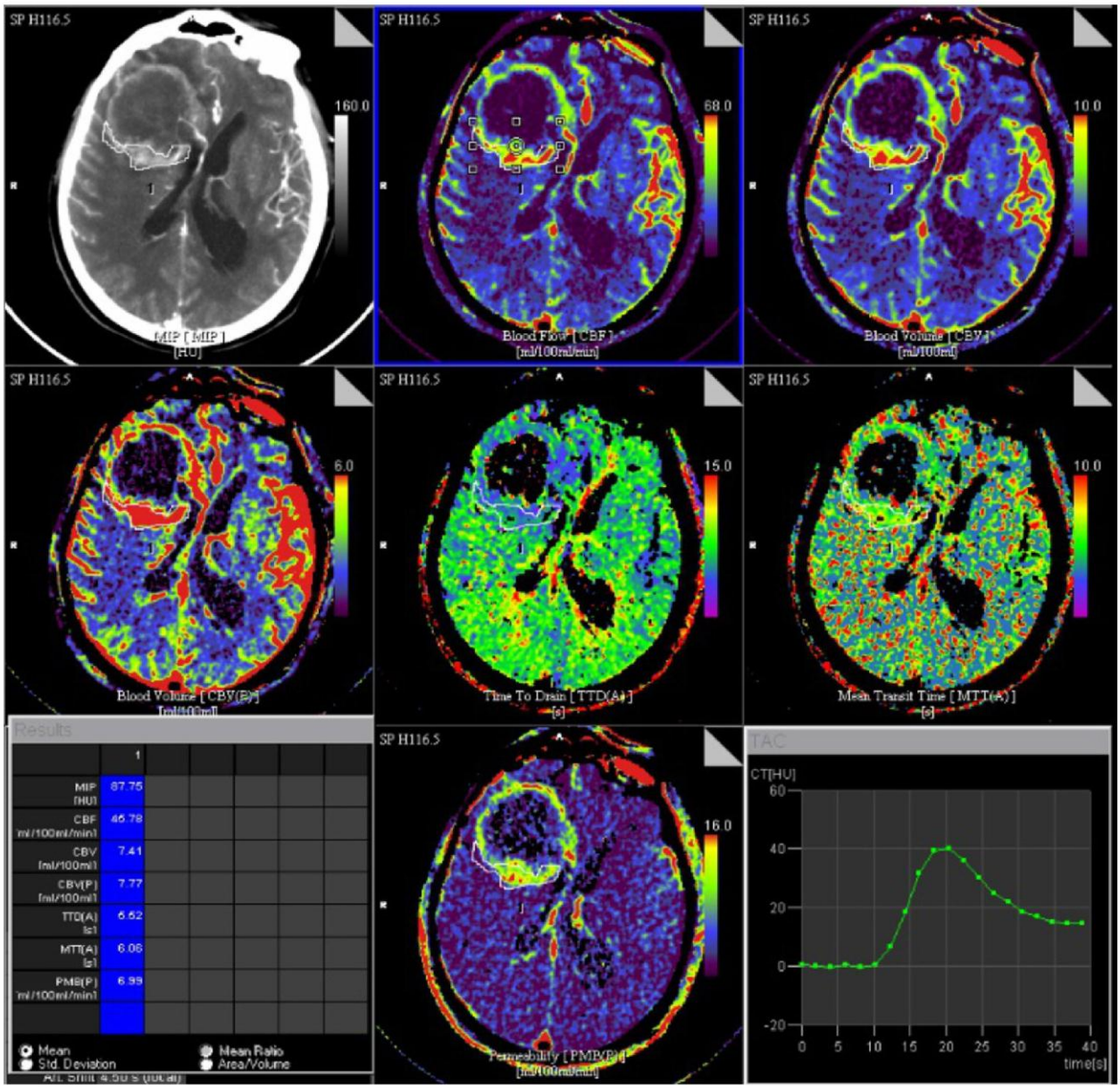

Fig. 3: 60 year old male patient with Mts of lung cancer in right frontal area. Histology: small-celled carcinoma. Perfusion parameters in solid part were: CBF 45.78 ml/100ml/min, CBV 7.41 ml/100ml, MTT 6.06 sec, PMB 6.99 ml/100ml/min.

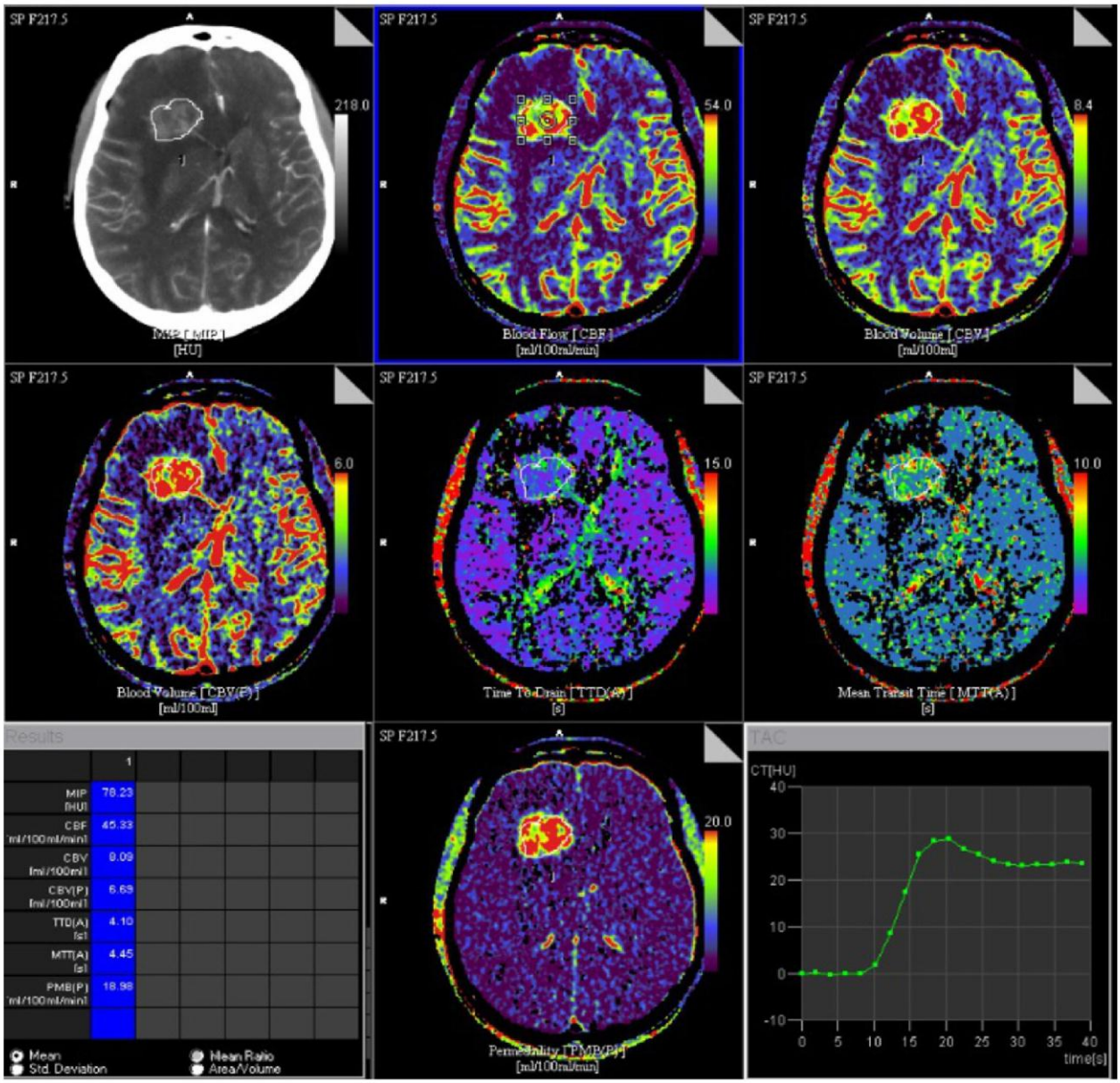

Fig. 4: 42 year old female patient with Mts of breast cancer in right frontal area. Histology: ductal carcinoma. Perfusion parameters in solid part were: CBF 45.33 ml/100ml/min, CBV 9.09 ml/100ml, MTT 4.45 sec, PMB 18.33 ml/100ml/min.

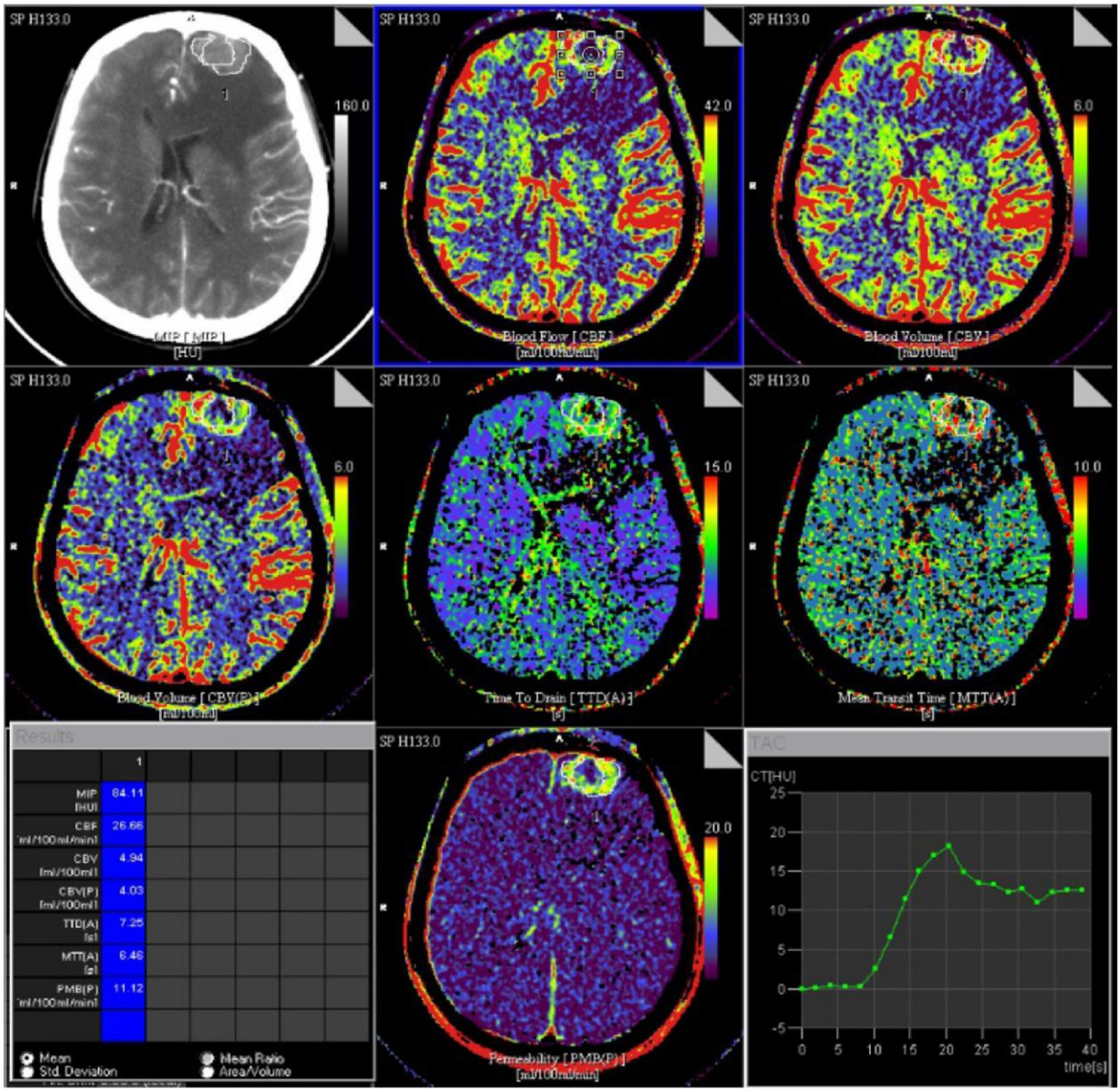

Fig. 5: 51 year old female patient with Mts of colon cancer in left frontal area. Histology: adenocarcinoma. Perfusion parameters in solid part were: CBF 26.65 ml/100ml/min, CBV 4.94 ml/100ml, MTT 6.48 sec, PMB 11.12 ml/100ml/min.

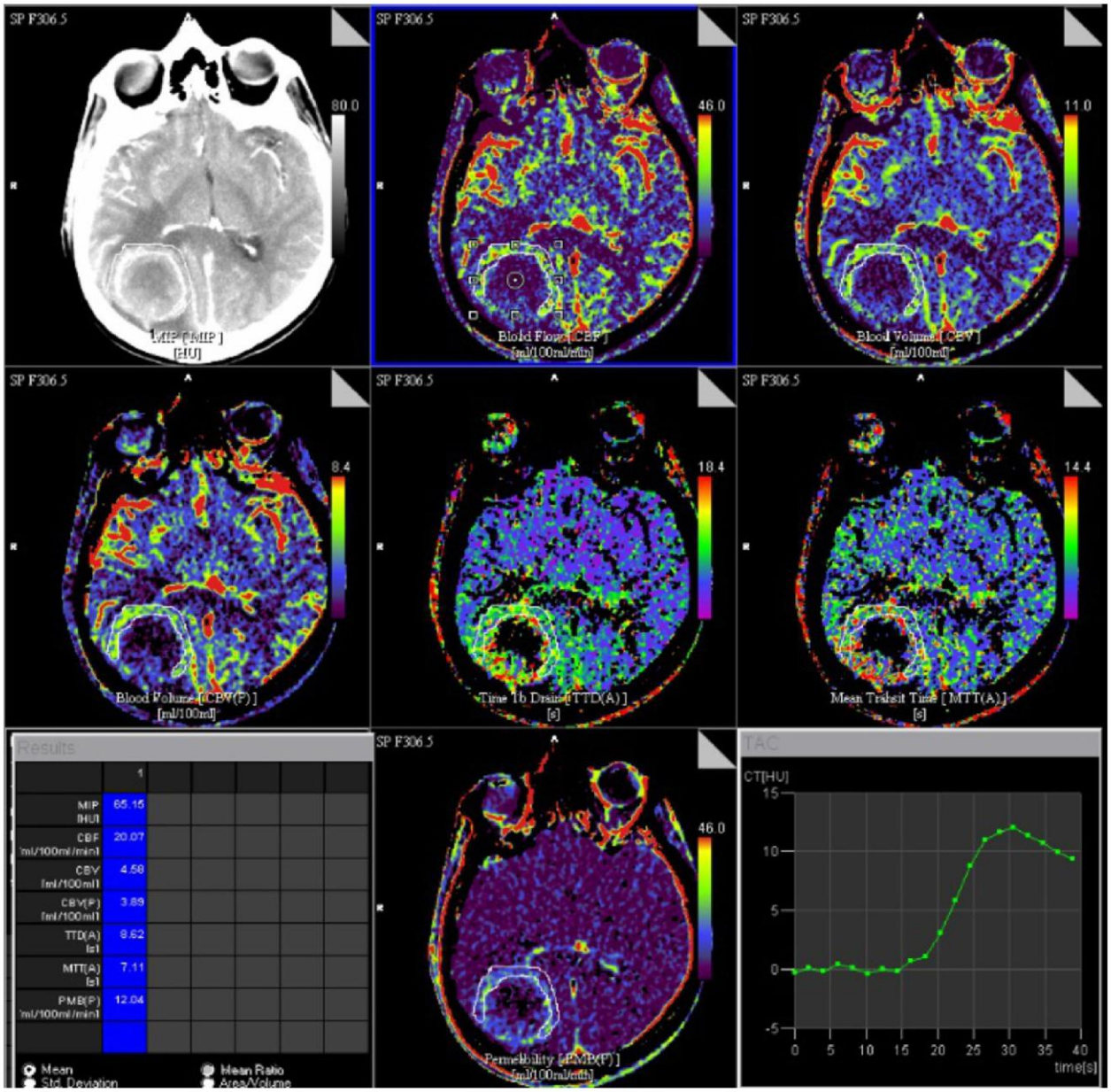

Fig. 6: 47 year old male patient with Mts of gaster cancer in right occipital area. Histology: adenocarcinoma. Perfusion parameters in solid part were: CBF 20.07 ml/100ml/min, CBV 4.5 ml/100ml, MTT 7.11 sec, PMB 12.04 ml/100ml/min.

Conclusion

The highest rates of perfusion parameters in solid part were observed in renal cancer (because of a severity of vascular network). Melanoma Mts had less values. There was no difference between cerebral metastases of lung or breast cancer. The lowest parameters were in cerebral metastases of colon and gastric cancer.

Perfusion parameters depend on the histology of intracranial lesions. CT perfusion parameters reflect a vascularity of brain metastases (Mts).The PCT may help to differentiate some secondary cerebral tumors various histology. It is particularly important when the primary source of cerebral metastases is undiagnosed. And date of vascularization is important for surgeons before an operation - to provide intraoperative hemorrhage.

References

1. Kornienko V.N., Pronin I.N. Diagnostic neuroradiology, 2006# p.425-462.

2. Pronin I.N.et al. CT perfusion in stereotactic biopsy of diffusion gliomas. Nevskii forum of radiology, SPb, 2005; 16-18.

3. Nabavi Darlus G., Cenic Aleska, Bennett J.D. CT assessment of cerebral perfusion: experimental validation and initial clinical experience. Radiology, 1999; 213: 141-149.

4. Bulakbasi N., Kocaoglu M., Somuncu I. Assessment of Diagnostic Accuracy of Perfusion MR

Imaging in Primary and Metastatic Solitary Malignant Brain Tumors. Am. J. Neuroradiol. 2005; 26:2187-2199.

5. Wintermark M., Smith W. S., Dillon W. P. Dynamic perfusion CT: Optimizing the temporal resolution and contrast volume for calculation of perfusion CT parameters in stroke patients. Am. J. Neuroradiol, 2004; 25:720-729.

6. Kornienko V.N., Dolgushin M.B. Complex diagnostics of brain metastases. Medical visualization, 2004; 3:89-96

7. Dolgushin M.B., Pronin I.N., Fadeeva L.M., Kornienko V.N. Perfusion computer tomography in differential diagnosis of brain metastases. Medical visualization, 2007; 4:100-106

Personal Information

Cancer Researce Center